A major dyke swarm in the Ogaden region south of Afar and the early evolution of the Afar triple junction

D. MÈGE[1,2,3]*, P. PURCELL[4], A. BÉZOS[2,3], F. JOURDAN[5] & C. LA[2,3]

[1]*WROONA Research Group, Institute of Geological Sciences, Polish Academy of Sciences, Research Centre in Wrocław, 75 Podwale St., 50449 Wrocław, Poland*

[2]*Laboratoire de planétologie et géodynamique, UMR CNRS 6112, Université de Nantes, 2 rue de la Houssinière, 44322 Nantes, cedex, France*

[3]*Observatoire des Sciences de l'Univers Nantes Atlantique (OSUNA, CNRS UMS 3281), Nantes, France*

[4]*P & R Geological Consultants, 141 Hastings St, Scarborough, WA, 6019, Australia*

[5]*Western Australia Argon Isotope Facility, Department of Applied Geology, Curtin University, GPO Box U1987, Perth, WA, 6845, Australia*

**Corresponding author (e-mail: daniel.mege@univ-nantes.fr)*

Abstract: Geological mapping in the Ogaden region of SE Ethiopia, integrated with aeromagnetic data, has revealed a large dyke swarm extending SSE more than 600 km from the southern Afar margin across the Somali Plate to the Ethiopia–Somalia border. $^{40}Ar/^{39}Ar$ age dating shows that emplacement occurred at 24–27 Ma, contemporaneous with early rifting and dyking in the Red Sea. Slab-pull forces generated at the Zagros subduction zone strained the lithosphere in the Afro-Arabian plate, and dyking began to extend south from the Red Sea at *c.* 27 Ma, extending across Afar, fed by a plume-related magma source, rather than the rift-related source prevailing along the Red Sea. Immediately south of the Afar margin, the dyke system was emplaced along the Precambrian Marda Fault Zone, and the continuation across the Ogaden may have been controlled by lithospheric weakness associated with a splay of the Marda Fault. We suggest that the Ogaden Dyke Swarm is a zone of crustal dilation continuing the Red Sea trend across the Horn of Africa and constituting the original third 'arm' of the Afar triple junction. Geochemical and geochronological analyses indicate that basaltic outpourings from the Ogaden Dyke Swarm flowed at least as far east as the Ethiopia–Somalia border and emanated from the same magma source as the Ethiopian flood basalts, which had erupted earlier at *c.* 30 Ma. Dykes are emergent only occasionally and are marked at the surface by linear sand-filled troughs varying from 2 to 20 m deep caused by tensional collapse above the dyke tip. Magnetic anomalies associated with the dykes vary in width up to 1 km and likely identify dyke zones.

Supplementary material: Geological map of the Marda Fault Zone and surroundings; argon dating analytical protocol and isotopic data corrected from baseline; petrographic description of representative samples of the Ogaden Dyke Swarm and analytical protocol used for geochemistry are available at http://www.geolsoc.org.uk/SUP18829

The continental-scale rifts of the Red Sea, the Main Ethiopian Rift (MER), and the Gulf of Aden meet in northern Ethiopia at the Afar triple junction (Fig. 1). The African and Arabian plates are in the early stages of separation along oceanic spreading centres in the Red Sea and Gulf of Aden, while the MER, now a segment of the East African Rift System, marks an earlier stage of continental rifting between the Nubian and Somalia plates. The evolutionary progression from MER to Afar to Red Sea to Gulf of Aden, though not without substantial complexity, offers considerable insight into the process of continental break-up.

The region has also been the site of extensive volcanism during the Tertiary. Following early (45–35 Ma) volcanic events in southern Ethiopia (Ebinger *et al.* 1993; George & Rogers 2002), voluminous outpourings of basaltic and acidic igneous material at about 31–28 Ma (Hofmann *et al.* 1997; Rochette *et al.* 1998) covered vast areas of Yemen and Ethiopia (Mohr 1975, 1983, 1991; Zanettin & Justin-Visentin 1975; Mohr & Zanettin 1988; Ukstins *et al.* 2002 and references therein), reaching a maximum thickness of about 3 km in one of the world's Large Igneous Provinces (LIP). Subsequently, large shield volcanoes developed on the

From: WRIGHT, T. J., AYELE, A., FERGUSON, D. J., KIDANE, T. & VYE-BROWN, C. (eds) *Magmatic Rifting and Active Volcanism.* Geological Society, London, Special Publications, **420**, http://doi.org/10.1144/SP420.7

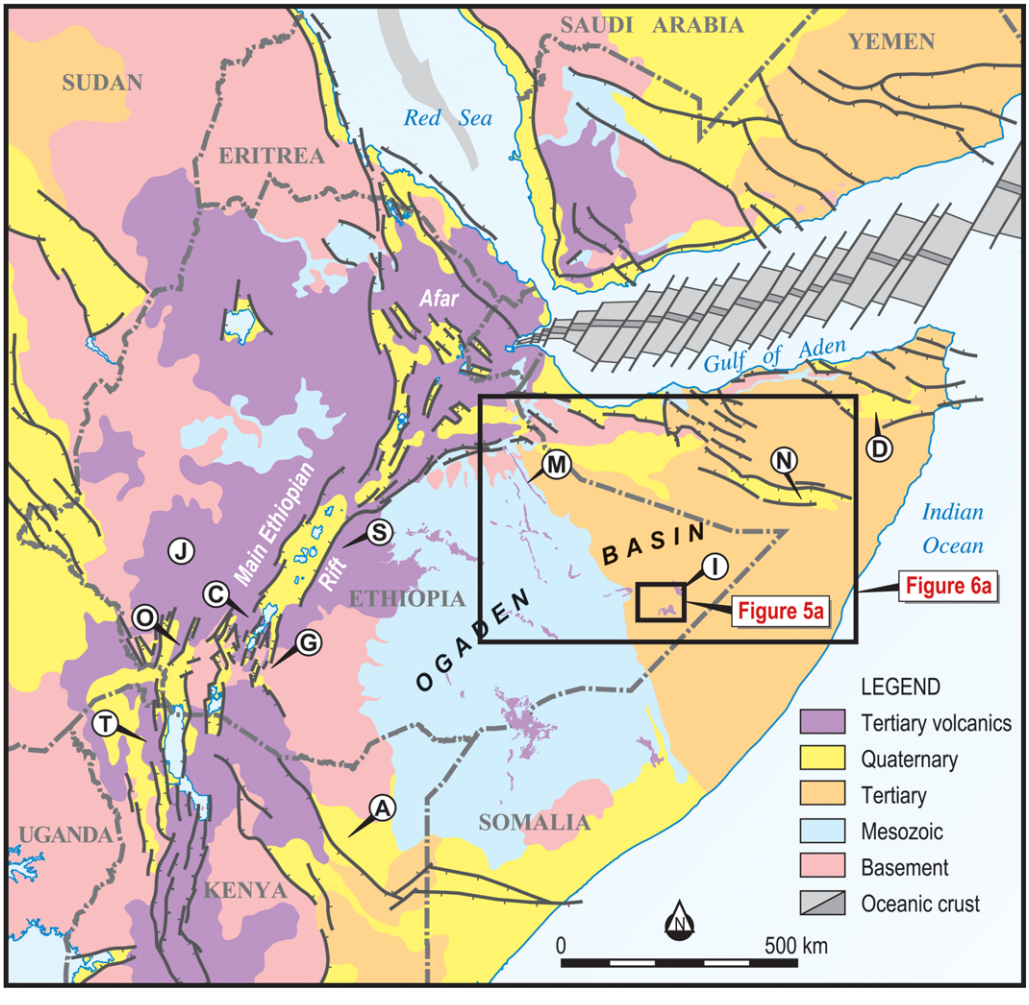

Fig. 1. Location map, Afar triple junction and surrounding region. A, Anza Rift; C, Chamo Graben; D, Darror Rift; G, Galana Graben; I, Ilbah Hills; J, Jemma area; O, Omo Rift area; M, Marda Fault Zone and volcanic line; N, Nogal Rift; S, Sagatu Dyke Swarm; T, Turkana Rift.

Ethiopian plateaux in the Miocene–Pliocene (Kieffer *et al.* 2004) while recent magmatism is confined to the MER and Afar. The structural and temporal relationship of this extensive magmatism to the process of continental rifting and break-up has been an important point of study for many years (Mohr 1978, 1983; White & McKenzie 1989; Baker *et al.* 1996*a*; Kenea *et al.* 2001; Wolfenden *et al.* 2004, 2005; Bosworth *et al.* 2005; Ukstins Peate *et al.* 2005; Pik *et al.* 2008; Rooney *et al.* 2013). Overall, the Cenozoic magmatism in the Horn of Africa has been variously attributed to a single plume (e.g. Mohr & Zanettin 1988; Hofmann *et al.* 1997; Ebinger & Sleep 1998; Burov & Guillou-Frottier 2005; Rooney *et al.* 2012), two distinct plumes (Orihashi *et al.* 1998; Rogers *et al.* 2000; George & Rogers 2002; Lin *et al.* 2005; Pik *et al.* 2006), or a single thermo-mechanical feature sampling two distinct mantle reservoirs (Nelson *et al.* 2012).

Our current work is focused on several aspects of the age and significance of the volcanism in SE Ethiopia. In this context, we note that any comparison of the timing of the main volcanism of Ethiopia/Yemen with the onset of Afro-Arabian rifting and break-up cannot be generalized across all elements of the Afar triple junction because the Gulf of Aden, Red Sea and MERs have very different structural histories (Fig. 2).

Lithospheric stretching and rifting commenced in the Gulf of Aden around 35 Ma (Watchorn

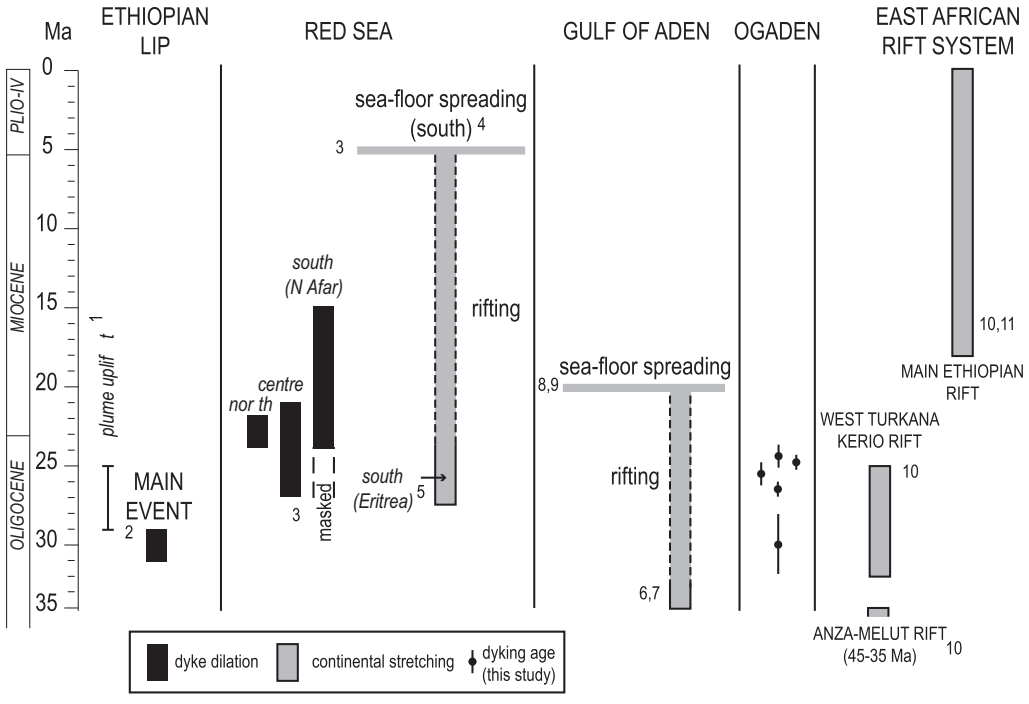

Fig. 2. Age of the main rifting and dyking events in the Red Sea, Gulf of Aden and Ethiopian Ogaden region. Numbers refer to: 1, Pik *et al.* (2003); 2, Hofmann *et al.* (1997); Rochette *et al.* (1998); Mège *et al.* (2010*b*); 3, Bosworth *et al.* (2005); 4, Cochran & Karner (2007); 5, Hughes *et al.* (1991); 6, Watchorn *et al.* (1998); 7, Autin *et al.* (2009); 8, Fournier *et al.* (2010); 9, Leroy *et al.* (2010); 10, Ebinger *et al.* (2000); 11, Pik *et al.* (2008).

et al. 1998; Autin *et al.* 2009) and was followed by oceanic spreading around 18 Ma (Fournier *et al.* 2010; Leroy *et al.* 2010). The beginning of continental stretching in the Red Sea has been dated at *c.* 29.9 Ma, based on biostratigraphy, in southern and central parts and *c.* 27.5 Ma in the north (Hughes *et al.* 1991; Bosworth *et al.* 2005). The accompanying dyking ranged in age from 27 Ma to 15 Ma, with the main dyking episodes from 27 Ma to 21 Ma (Sebai *et al.* 1991; Zumbo *et al.* 1995; Bosworth *et al.* 2005). Seafloor spreading started at 5 Ma in the southern part of the Red Sea, but there is no evidence of spreading in the north (Cochran & Karner 2007). The MER history is very different (Bonini *et al.* 2005); rifting did not commence at the southern end until *c.* 18 Ma (Morley *et al.* 1992; Ebinger *et al.* 2000) or even *c.* 20 Ma (Bosworth *et al.* 2005; Pik *et al.* 2008), and not until 10–11 Ma (Wolela 2004) at the northern end. Moreover, these segments did not amalgamate and propagate northwards into Afar as the third arm of the triple junction until *c.* 5 Ma (Bonini *et al.* 2005). Whatever tectono-magmatic links might have existed between the Oligocene volcanism and the Gulf of Aden and Red Sea arms of the Afar triple junction, they did not apply to the MER arm, which did not exist at that time.

A better understanding of the distribution and age of volcanics on the Somalia Plateau to the SE of the MER and Afar should assist efforts to understand the tectono-magmatic evolution of the broader region. The marked asymmetry of the volcanism along the MER, with much thicker and more extensive units on the Abyssinian Plateau on the western side of the rift, has long been noted and is clearly evident on the published maps of Cenozoic volcanic rock distribution in the African Horn (including Fig. 1 in this paper). The thickness of the flood basalts on the Abyssinian Plateau, the abundance and geometry of feeder dykes north and west of Lake Tana, and the co-incident regional Bouguer gravity negative anomaly have led to speculation that the initial centre for magmatism may have been in the Lake Tana area (Chorowicz *et al.* 1998; Mège & Korme 2004*a*). The Abyssinian Plateau volcanics, as well as the volcanics in the Afar, have been studied in greater detail than the southeastern volcanics (see references in Mohr & Zanettin 1988 and Mège & Korme 2004*a*), which have been mapped in detail only locally. The

volcanics on the Somalia Plateau are over 1500 m thick along the southeastern escarpment (Juch 1975) but thin rapidly to the east and south, and most outcrops are less than 50 m thick. It remains unclear why the volcanism is relatively diminished along this southeastern MER/Afar margin.

Extensive studies of aerial and satellite imagery, coupled with helicopter-supported and road-based field surveys in 2005, 2008, 2011 and 2014, have provided a new map of the volcanic outcrops in SE Ethiopia in the region commonly called the Ogaden. We report the results of geological mapping and aeromagnetic data, which have revealed a dyke swarm extending SSE more than 600 km from the southern Afar margin across the Somali plate to the Ethiopia–Somalia border. $^{40}Ar/^{39}Ar$ age dating shows that initial emplacement of the dykes post-dated the flood basalt eruptions at 31–28 Ma and ended at the onset of the 'regional Red Sea dyking event' at 24 Ma (Bosworth *et al.* 2005). Geochemical and geochronological analyses indicate that this Ogaden Dyke Swarm was a source for lavas similar to the flood basalts, extending as far east as the Ethiopia–Somalia border, in regions remote from the Afar and MER. We suggest that the Ogaden Dyke Swarm is a zone of crustal dilation continuing the Red Sea trend across the Horn of Africa and constituting the original third 'arm' of the embryonic Afar triple junction.

The Ogaden dyke swarm: identification

Geological observations

Mapping of the volcanic outcrops in SE Ethiopia has been based primarily on Landsat Geocover mosaics 1990 and 2000, available at Global Land Cover Facility (http://glcf.umd.edu/). Geocover 1990 has a resolution of 28.5 m/pixel and combines Landsat spectral bands 7 (red), 4 (green) and 2 (blue). This processing is especially well adapted to geological interpretation where the vegetation cover is absent or limited. Geocover 2000 combines these bands with the panchromatic band of sensor Landsat Enhanced Thematic Mapper Plus (ETM+) and then re-samples at the panchromatic band resolution of 14.25 m/pixel. Advanced Spaceborne Thermal Emission and Reflection Radiometer (ASTER) visible near-infrared (VNIR) image coverage (15 m/pixel), available throughout the Ogaden, has also been used locally. Observations were refined using metre- to decimetre-scale resolution multispectral imagery available in Google Earth®.

The most discriminating dataset for identification of basaltic rocks throughout the Ogaden has proved to be Geocover 1990. Basalt outcrops are identified as distinctive deep blue patches. Clays produced by basalt alteration have the same spectral signature but can be distinguished by their topography: the basaltic hard-rock outcrops form prominent and distinctive hills rising above the monotonous SE-dipping surface of the Ogaden, while basaltic clays are observed to fill flat pans, generally subcircular in shape.

Mège *et al.* (2015) have studied the geomorphology of the volcanic outcrops throughout the Ogaden to deduce some geodynamic implications. The observations discussed in this paper relate mainly to key outcrops in two areas linked to the Ogaden Dyke Swarm, the Marda Range near Jijiga and the southeastern Ogaden (Fig. 3). Helicopter-supported field work in the eastern and southern Ogaden was conducted in March and September 2008. Security conditions in the field restricted the time available on the ground for detailed measurements and sampling, but the helicopter provided access to otherwise inaccessible areas to enable observation and sampling of many remote areas for the first time. Fieldwork in the Marda Range area was conducted by vehicle in December 2005 and February 2011 and 2014.

Volcanic deposits in SE Ethiopia form broad volcanic plateaux, linear outcrops, isolated hill complexes, and meandering ribbons of exhumed palaeovalley basalt fill. The best known volcanic outcrop in the region is in the Marda Range, a chain of uplifted and eroded hills of Jurassic limestone capped by an elongate basaltic layer trending SSE from Afar to the central Ogaden parallel to the first-order drainage pattern. The basalt cap forms a prominent dark lineament on satellite imagery, 150 km long and up to 2 km wide.

The uplifted Mesozoic sediments of the Marda Range, the capping basalt layer and the underlying foliated Precambrian are referred to, in tectonic terms, as the Marda Fault Zone. Purcell (1975, 1976), following Gouin & Mohr (1964), referred to it as a Precambrian mylonite zone and reports its reactivation several times during the Phanerozoic. This 'volcano-tectonic' line was first recognized in 1920 (Brown 1943) but remains poorly understood. It is a topographic and geological divide between the eroded Mesozoic carbonates and evaporites of the western Ogaden and the sand plains of Tertiary sediments in the east (Purcell 1981*a*). A fault zone, downthrown 200+ m to the east, is indicated by surface geology and stratigraphic boreholes on the eastern side of the northern Marda Range, and seismic data suggest the throw may be 2 km or more (Maxus Ethiopia 1993). The Marda lineament can be projected to the NNW into the Erta Ale axis and the Red Sea, and to the SW into transform zones in the oceanic Somali Basin. This has prompted speculation about the

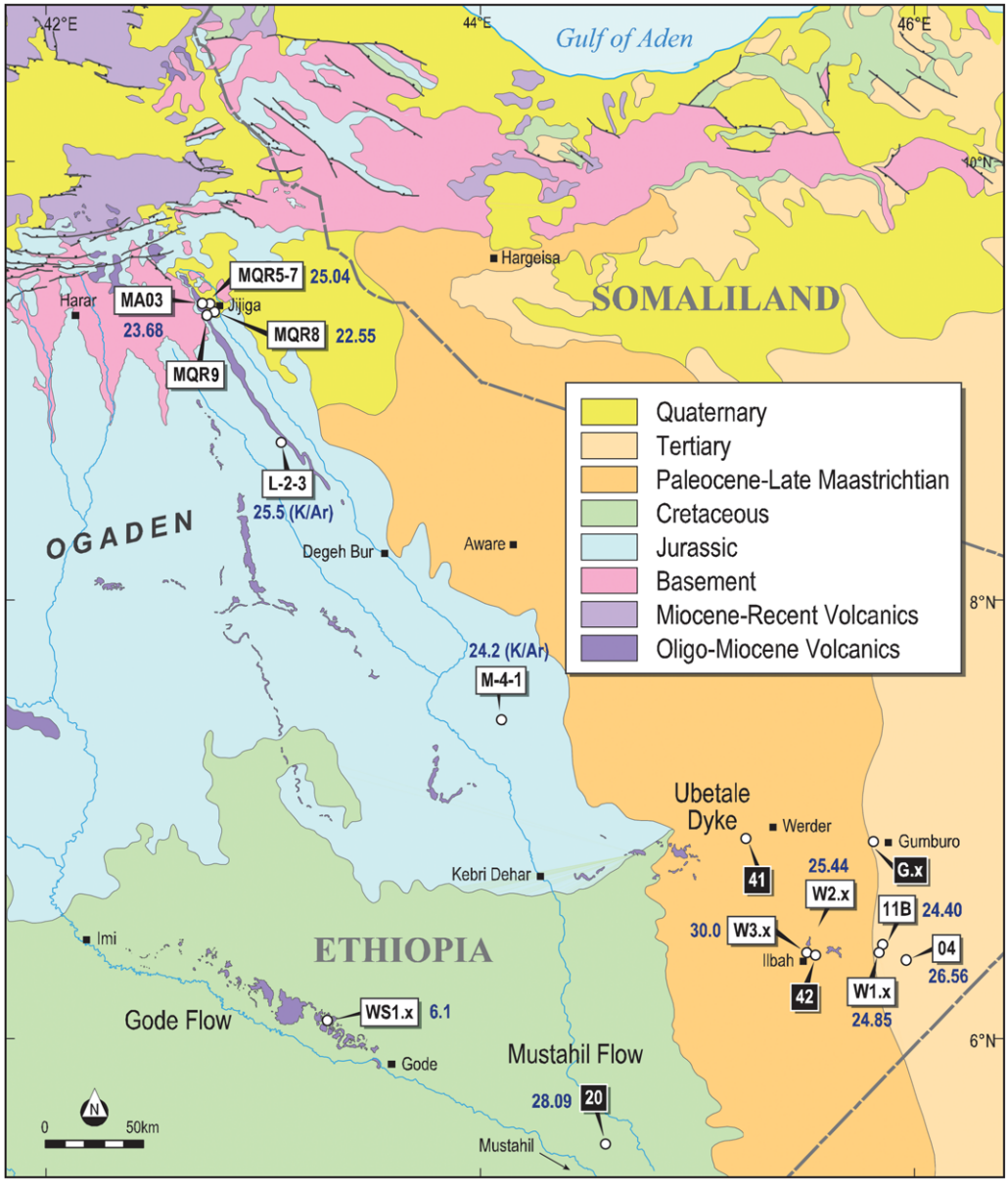

Fig. 3. Simplified geological map of the Ogaden showing sample sites, their $^{40}Ar/^{39}Ar$ age, and their geochemical group as discussed in the text. Sites of samples having $(Sm/Yb)_N > 2.7$ (geochemical Group 1) have a black label; sites with samples having $(Sm/Yb)_N < 2.7$ (Group 2) have a white label. Age uncertainty is given in Table 2. Sample IDs with '.x' are for a group of samples collected at the same site. K–Ar ages obtained by Teledyne Isotopes for Maxus Ethiopia (1993) are also shown. Uncertainty for those ages is 1.3 Ma.

controlling influence of the zone in the geodynamic evolution of both the Horn of Africa and the adjacent Indian Ocean (Wood 1979; Boccaletti *et al.* 1991; Shackleton 1996).

The Marda Range has also been interpreted as a graben structure, presumably inverted, extending SE into Somalia as the Hiraan Rift (Bosellini 1989), also called the Wabe Shebele Rift (Rapolla *et al.* 1995), and suggested to be of Permian to Jurassic age. This 'rift' is reported to be defined on gravity data and inferred from the drainage system (Sommavilla *et al.* 1993) but neither gravity nor

seismic data recorded in this area in the 1980s (Shell Internationale Petroleum Mij B. V. 1988) show any indication of a major NW–SE-trending rift structure.

In a regional context, it is noteworthy that the zone of tilted fault blocks along the southern Afar margin terminates close to (if not at) the Marda Fault Zone. Here, Precambrian basement and Mesozoic sediments replace Quaternary volcanics and alluvium as the defining outcrops of the Afar floor (Figs 1 & 3). The role and significance of this 'continental' block (Kazmin 1972), variously called the Aisha Block (e.g. Garfunkel & Beyth 2006) or Ali Sabieh Block (e.g. Manighetti *et al.* 2001), in the tectonic development of the Afar triple junction, notably as a constraint on past plate kinematics, remains poorly understood. Its contact with the Somalia Plate is seismically active (Ruegg *et al.* 1981), but the nature of this contact is debated (Audin *et al.* 2004; Garfunkel & Beyth 2006; Bottenberg 2012).

In the area studied, the Marda basaltic layer, about 200 m thick, consists of a number of thick, columnar basaltic flows (Fig. 4a). At the Marda Pass, where the Harar/Jijiga road cuts across the Range, excellent local exposures reveal an undulating erosional contact between the basal Marda lava flow and the underlying Jurassic Hamanlei Formation limestones, suggestive of a palaeovalley filling flow, as has occurred elsewhere in the Ogaden (Mège *et al.* 2015) and southern Somalia (Abdirahim *et al.* 1993). The Marda lava flows may have filled, and substantially overflowed, a linear ancestral channel of the Fafan River, now flowing 10 km to the west of, and parallel to, the Marda Range (Mège *et al.* 2015). There is no evidence of dykes feeding the Marda lava flows within the limited outcrop area, but recently-cut quarries in the Jurassic limestones 200–400 m away on the eastern side of the Marda Range, at the Marda Pass, reveal voluminous subsurface basaltic intrusions of irregular geometry, ranging to over 10 m in width and from which narrow dykes (thickness <1 m) have propagated upwards under low deviatoric stress (Fig. 4b). These quarry exposures reveal for the first time the intrusive activity in the Marda Range.

In the southeastern Ogaden, satellite images and Shuttle Radar Topography Mission (SRTM)-3 topographic data reveal several complexes of volcanic hills (e.g. Fig. 4c) and widespread NW–SE trending lineaments (Fig. 5a), many of which were visited during fieldwork in 2008. The lineaments are shallow depressions, 100–300 m wide and about 2–20 m deep, marked by contrasting vegetation density (Fig. 5b) and occasional calcrete exposures (Fig. 5c). Calcrete, chert and duricrust fragments are common along the trough margins and are present, though less common, within the troughs. Similar depressions, though ovoid in shape, are widespread in eastern Ogaden, where they are considered the result of dyke-parallel fracturing similar to rift-related fracturing in Afar (Wright *et al.* 2006) and along the Red Sea margin (Baer & Hamiel 2010), followed by hydrothermal alteration and limestone and/or gypsum dyke-parallel karstification (Mège *et al.* 2008; Mège & Purcell 2010). Many of these lineaments coincide with high-frequency linear magnetic anomalies, as discussed further below.

While there is otherwise little field evidence of volcanic activity along the troughs, several basaltic hills are located along the trend of these prominent surface lineaments. The hills (Ilbah Hills, located on Fig. 1) are generally broad mounds covered with rounded basalt cobbles and pebbles, and actual outcrops are few and scattered. The topographic linearity of the hills, and the lineaments observed on satellite imagery, suggest the presence of emergent dykes, but the poor quality of the outcrops makes identification difficult. The most prominent dyke identified, at Raqo Hill (Fig. 4c), was confirmed from its chilled margins (Fig. 4d). It is highly vesicular, with a similar structure to that of the surrounding lava flow, indicating cooling at or near the surface. Near the village of Ubetale, a linear exposure of basalt, 3.5 km long and 260 m wide with sharp boundaries (Fig. 4e, f), is clearly observed on satellite imagery. This low topographic mound is located along a linear magnetic anomaly (Fig. 6d), suggesting that it is the surface manifestation of a dyke, but there are no outcrops to confirm this by way of evidence of chilled margins, for instance. The volcanics appear to be surrounded by sediments. Dykes of this width (260 m) are common in continental shields where kilometres of overlying rocks have been removed (Halls & Fahrig 1987) but unknown at such a shallow emplacement depth, not more than hundreds of metres, based on the maximum thickness of the sedimentary cover that may have been eroded (e.g. Bosellini 1989). Consequently, we suggest that the original Ubetale dyke is much narrower than 260 m and, while not exposed, has locally erupted with the outpoured basalts filling a broader fracture-bound depression produced as a result of the dyke emplacement.

Prominent among the Ogaden volcanic hills are a series of long (>100 km) meandering basalt hills, which are topographic inversions of the palaeoriver-channel-filling flows. Two of the main flows were sampled during the 2008 helicopter survey to investigate whether similarities of age and composition of the basalts would confirm the Ogaden Dyke Swarm as the source. The Mustahil lava flow, described here for the first time, is located NW of Mustahil town in the southern Ogaden (Fig. 3). It is 90 km long, but with eroded 'gaps' between

the basaltic remnants (Fig. 4g), and originally flowed in a succession of gently meandering narrow valleys in the Cretaceous Mustahil Formation limestone. The Gode lava flow (Fig. 4h), easily traced for more than 200 km, originally flowed down the major meandering palaeo-Wabe Shebele canyon and appears to have locally overflowed the river channel to form overbank basaltic pods.

Identification on aeromagnetic data

Field mapping and drilling at Gumburo-1 (Fig. 3) confirmed the presence of intrusive and extrusive magmatism in the Ogaden (Straub 1958), but it was the aeromagnetic data that provided the first indication of a dyke system in the region. Sinclair Petroleum (1950) noted that their aeromagnetic survey in the eastern Ogaden 'revealed several areas of high excessive magnetic anomalies indicating near-surface igneous bodies … generally confined to linear belts …' (Sinclair Petroleum 1950).

The first aeromagnetic survey over the Marda Fault Zone was flown by Whitestone Petroleum in 1976 (Geosurvey 1977) at a constant barometric altitude of 1830 m using a Geometrics G803 proton procession magnetometer with north–south-oriented lines 2.5 km apart and tie lines at 10 km spacing. The magnetic field is dominated by a broad, NE-trending negative anomaly of about 500 nT magnitude, with superimposed local anomalies of mainly NE and NW trends, and cut by linear NW–SE-trending high-frequency anomalies (Fig. 6). The broad anomaly is closely co-incident with a major gravity high (Purcell 1975) and is caused by deep (5–6.5 km) intra-basement density and susceptibility changes: the superimposed local anomalies are caused by bodies, possibly volcanic sills and intrusions, at subsurface depths of about 300–600 m. Long linear anomalies, which are particularly clear on the second-vertical-derivative map (Fig. 6), have been interpreted as two groups of very shallow dykes, one of normal polarity and the other reversed (Hunting Geophysics, in Geosurvey 1977), possibly indicating two periods of injection. The scale of these linear magnetic features, 30–60 km long and 1–2 km wide, suggests they mark complex intruded fracture zones, but the high survey elevation (700–800 m above ground) and wide line spacing precludes detailed definition of the zones or identification of individual bodies within them. It is also possible that the linear magnetic anomalies are related to shallow thick lava flows overlying narrower feeder dykes, similar to the main lava flow exposed in the quarries at the Marda Pass. In either case, the anomalies clearly mark the southeastward continuation of the Marda magmatism beyond the extent of the basaltic outcrops. A northward extension beyond the Marda outcrops has been noted previously by Shachnai (1972), who reported dykes and sills down-faulted by ENE-trending faults where the Marda Fault Zone intersects the southern Afar escarpment.

Modern high-resolution aeromagnetic data (UTS Geophysics 2008) over the SE Ogaden were obtained by Pexco Exploration (East Africa) NV in 2008 in a survey flown by UTS Geophysics using a Geometrics G822A caesium vapour total field magnetometer. Survey lines were flown on a bearing of 045° on a 1 km spacing with tie-lines flown at a 5 km spacing at a bearing of 135°. Average terrain clearance was 55 m, and the high resolution dataset provided detailed information on the surface and near-surface volcanics.

A reduced-to-pole (RTP) image of the total magnetic intensity data, released to the senior author through a collaborative arrangement with the University of Nantes, is shown on Figure 6. (The survey location is very near the magnetic equator, and the reduction-to-pole is an approximation.) The dominant features are (a) a swarm of linear high-frequency anomalies trending in a general NW–SE direction and (b) areas of high-frequency anomalies, commonly showing a central meandering anomaly pattern, both superimposed on broad low-frequency anomalies relatable to the deep Precambrian basement complex. The linear high-frequency anomalies extend from the southeastern end of the Marda Fault Zone (Fig. 6b) to the Ethiopia–Somalia border (Fig. 6c, d) and are interpreted as dykes. The anomalies are mainly of normal polarization (positive on the RTP), but several show a reverse negative polarity, as previously noted along the Marda Fault Zone (Hunting Geophysics, in Geosurvey 1977). There is no apparent distribution pattern to the normal v. reverse polarity of the dykes. Approximately 40–46 dykes and dyke segments can be seen, the number varying with a subjective interpretation of continuity: 15 trend WNW–ESE, about 13 trend NE–SW, 4 are intermediate between these trends, and 11 dyke segments trend almost east–west. The dykes vary in length from about 15–20 km to over 140 km, given that several extend beyond both the eastern and western boundaries of the survey area. A comparison with dyke swarms observed at deeper levels in the crust (e.g. Mège & Korme 2004*b*) and dyke emplacement mechanics (e.g. Schultz *et al.* 2008) suggests that there are likely many smaller dykes within the swarm that are not resolved by available data. In the absence of susceptibility data, precise computation of depth or width is not possible, but some of the dykes are at or very near the surface while others appear to be at depths of 200–600 m. The different polarities and trends support the

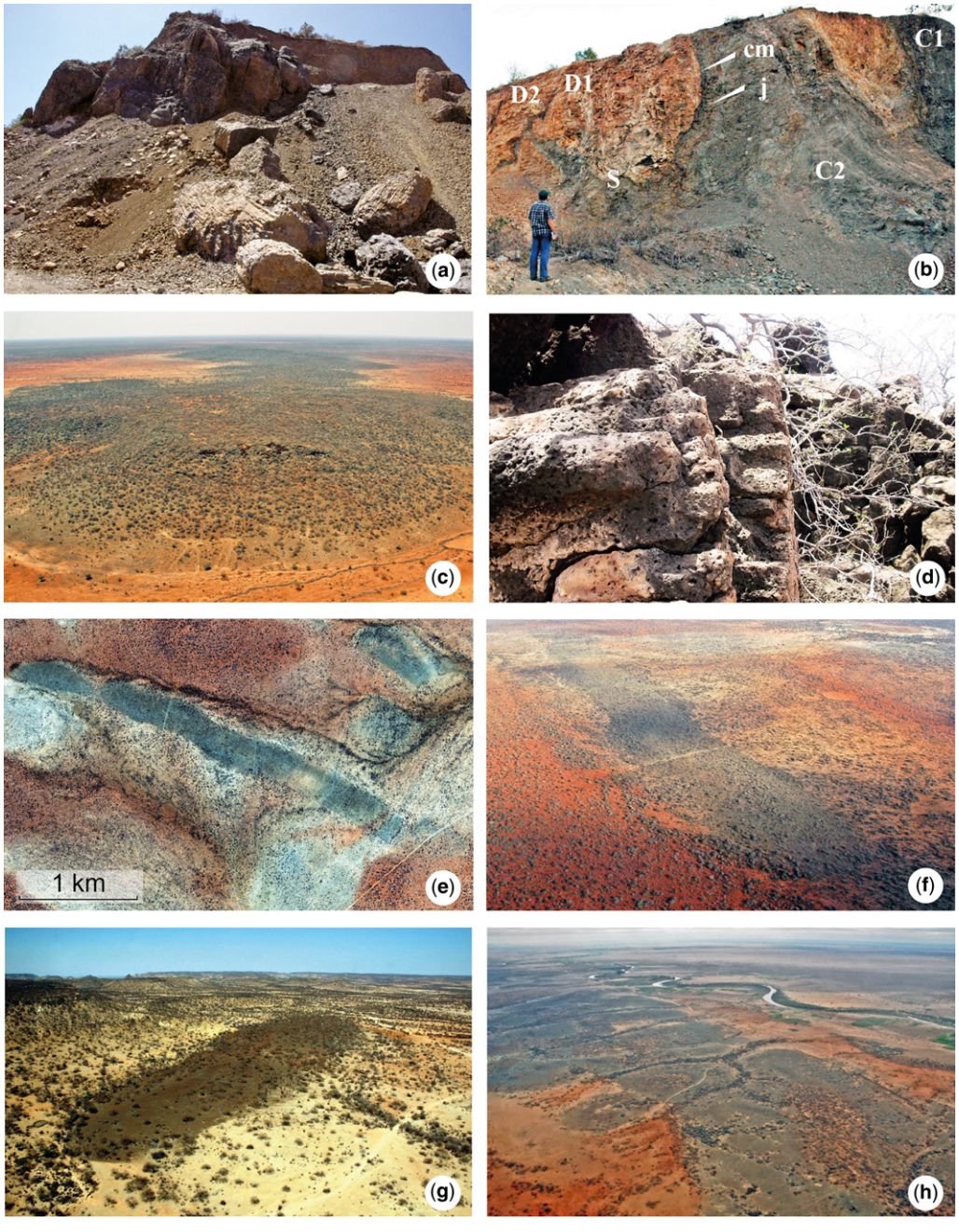

Fig. 4. Satellite, aerial and field photographs of selected sites (all located on Fig. 3). (**a**) Field view of a thick basaltic flow atop the Marda Range at sample MQR9 location. The cliff is more than 30 m high. (**b**) Field view of subsurface basaltic intrusions on the eastern side of the Marda Pass in the northern Marda Range. The contact zone between the intrusions and the host rock is densely jointed (j) and the intrusions display chilled margins (cm). Conical intrusions C1 and C2 have similar dimensions. C1, C2, sill S and dykes D1 and D2 were all injected from the same larger intrusive body cropping out elsewhere in the quarry. D1 and D2 do not display any chilled margins (not seen here), suggesting that the host rock was already warmed by the intrusion when the dyke propagated. The host rock was cool enough to be baked at the dyke contact. Samples MQR6 and MQR7 were collected in dyke D2. (**c**) Aerial view of dyke at Raqo Hill where sample 11B was collected. The dyke overlies a linear magnetic anomaly.

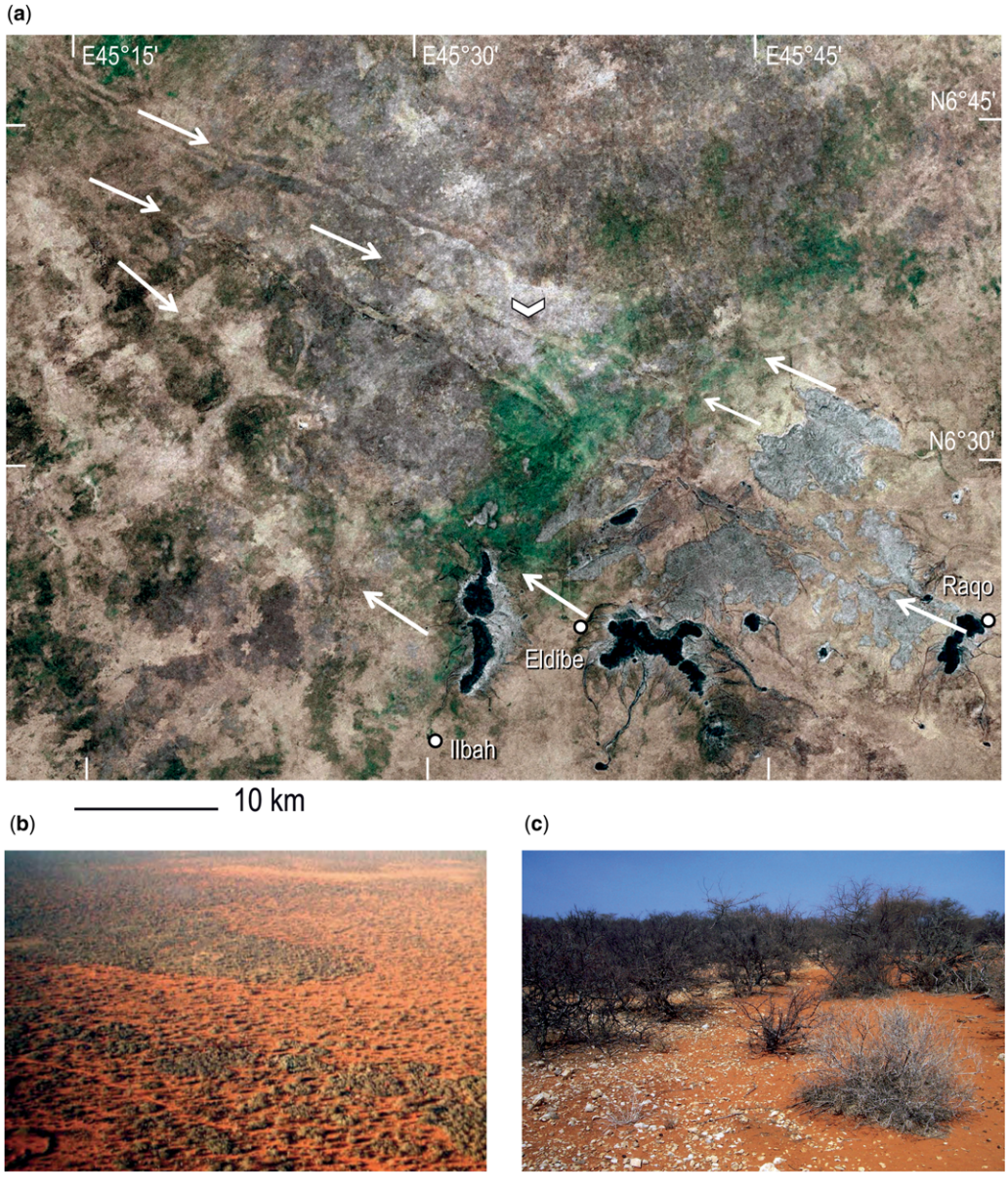

Fig. 5. The dyke-swarm lineaments. (**a**) Satellite image of eastern Ogaden showing linear troughs, several of which are co-incident with linear magnetic anomalies. The white arrows point to the linear troughs. The white arrowhead indicates the viewing direction of the aerial photograph in (b). (**b**) Aerial view of the linear trough displayed in (a); view is to the south. (**c**) Ground view of the 'contact' between this trough (on the right) and its margins. The white cobbles are calcrete and chert.

Fig. 4. (*Continued*) (**d**) Field view of the altered chilled margin of the Raqo dyke. Note the large number and size of bubbles, which denote very shallow depth of cooling. (**e**) GeoEye image of the Ubetale Dyke where sample 41 was collected. Note a possible second dyke in the upper right corner of the image. North is at the top of the image. (**f**) Aerial view of the same dyke (field view would display cobbles and pebbles only). (**g**) Aerial view of the Mustahil lava flow (sample 20). (**h**) Aerial view of the Gode lava flow along which samples WS1.2 and WS1.3 were collected. The flow occupies a palaeochannel of the Wabe Shebele, which is seen in the background on the right.

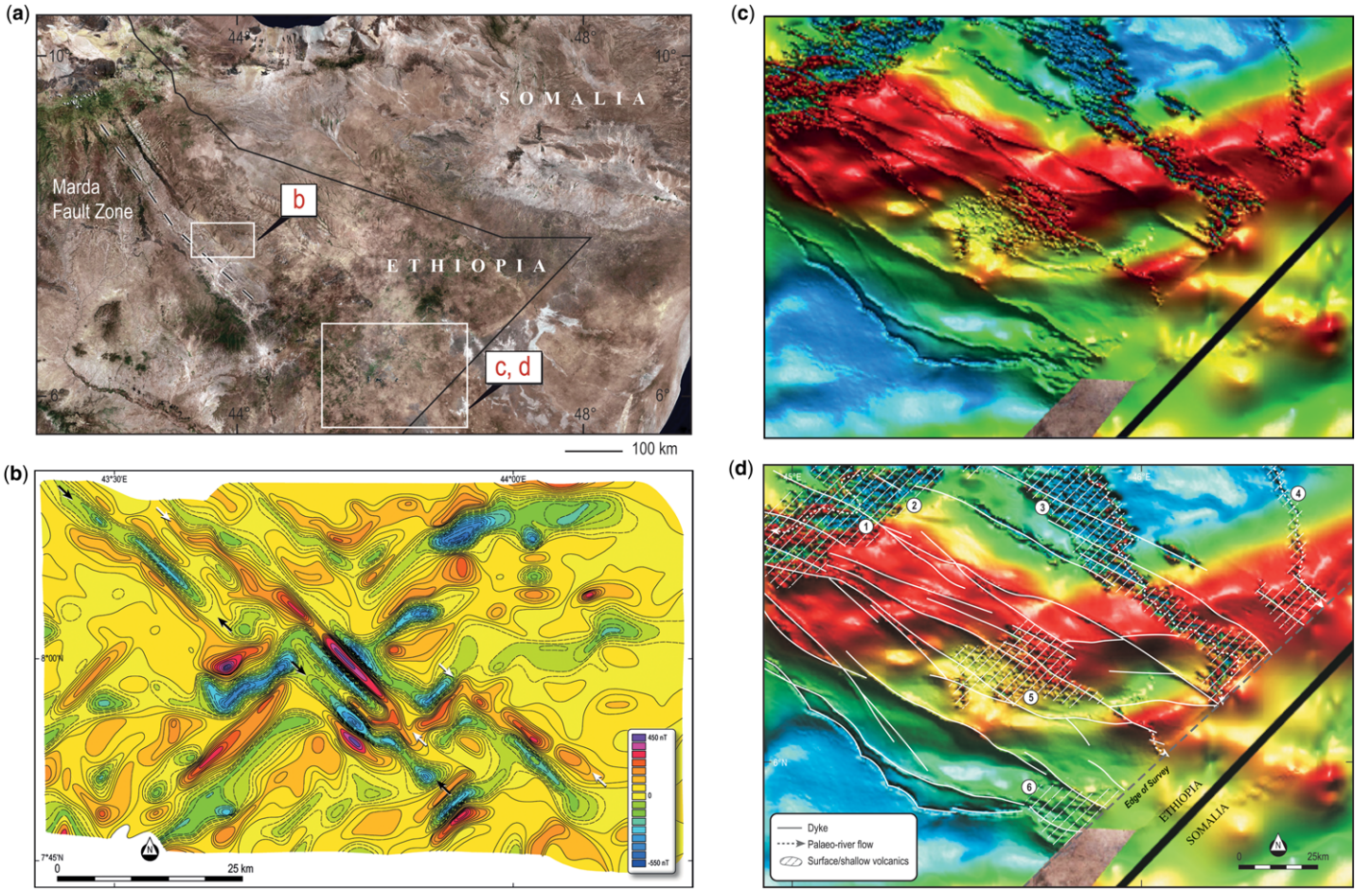

Fig. 6. (**a**) Satellite mosaic of the Ogaden showing the location of the Marda Fault Zone and the magnetic maps displayed in (b), (c) and (d). (**b**) Whitestone second vertical derivative magnetic map across the central Marda Fault Zone (Geosurvey 1977). The normal and reversely magnetized dyke-related anomalies are shown by black and white arrows, respectively. (**c**) Pexco first vertical derivative Reduced-to-Pole (RTP) magnetic map in eastern Ogaden. (**d**) Geological interpretation of (c). Numbers refer to features discussed in the text. Dyke-related anomalies are marked in white. Note the dimensions of lava flows indicated by the magnetic data, in comparison to the limited outcrops, shown on Figure 3.

suggestion that several episodes of dyke injection are involved. Many of the dyke-related magnetic anomalies coincide precisely with the lineaments observed on satellite imagery and elevation models, showing the link between surface and subsurface structures. The presence of elongate shallow troughs above dykes identified from magnetic data and 3D seismic data has been described in the southern North Sea Basin by Wall *et al.* (2009).

Six areas of surface to near-surface volcanics can be seen on Figure 6d: the Ubetale Dyke volcanics (1), SW- and SE-trending areas in the north (2 and 3, respectively), a narrow sub-meridional ribbon in the NE (4), a central area around the Ilbah Hills outcrops (5) and an area in the SE (6). The dykes are clearly seen to pass through all these areas. Within each of the three northern areas, a meandering ribbon of high amplitude anomalies can be seen: this is especially clear in the larger NW–SE-trending complex (3 on Fig. 6d). It is likely that these represent lava flows down old river channels, similar to the outcrops of meandering hills elsewhere in the Ogaden (Mège *et al.* 2015). The broader areas of volcanics flanking the meandering complexes might have been formed by overbank lava flows but could also have been fed by the dykes. There is a markedly different magnetic signature to the channel-related anomalies and the broader anomalous area, and they may not be contemporaneous.

We interpret the new magnetic data as completing the evidence for a major dyke complex, the Ogaden Dyke Swarm, extending some 600 km from the Afar margin to the Somalia border. Dykes are observed in outcrop at the Afar margin, along the Marda Range and in the eastern Ogaden, and surface lineaments and aeromagnetic anomalies reveal the continuity of the dyke complex in intervening areas. The Marda Fault Zone has historically been projected SSE to the Ethiopia–Somalia border along the Wabe Shebele valley, where a pronounced lineament on satellite imagery coincides with the contact of outcropping Mesozoic and Tertiary sediments (Black *et al.* 1974; Wood 1979). The more southeasterly trend manifest in the faulted Jurassic outcrops in the Marda Fault Zone south of 8° N has always seemed in conflict with that SSE projection but is now seen to be quite precisely aligned with the Ogaden Dyke Swarm. A prominent NW–SE-trending negative gravity lineament extends from those Marda outcrops along the trend of the Ogaden Dyke Swarm and appears to be primarily related to structures within the Precambrian basement (Purcell 1981*b*). We interpret this to mean that the Marda Fault splays into several faults south of 8° N, but we recognize the possibility that the historical projection SSE along the Wabe Shebele might be incorrect.

Argon dating of the Ogaden Dyke Swarm

We selected 14 fresh-looking basalt samples from, or seemingly related to, the Ogaden Dyke Swarm from the Marda Range and the southeastern Ogaden (Fig. 3 and Table 1) for $^{40}Ar/^{39}Ar$ dating. Groundmass particles were separated for 11 samples, plagioclases were separated for one sample, and two samples were split to provide both groundmass and plagioclase separations. The results are presented in Table 2 and Figure 7. Uncertainties on the ages are given at 2σ.

We obtained seven plateau ages. Five robust ages were obtained from the groundmass samples, of which four range from 23.68 ± 0.54 Ma to 26.56 ± 0.45 Ma, with *P*-values ranging from 0.44 to 0.98, and one is much younger, 7.46 ± 0.47 ($P = 0.22$). Two plateau ages have been obtained from plagioclase samples; 30.0 ± 1.9 Ma ($P = 0.72$) and 6.10 ± 2.4 Ma ($P = 0.75$). The 6.10 Ma age was initially considered anomalous, given the unexpected age and high uncertainty at 2σ, but has been validated by the 7.46 Ma age sample from the same site. Another groundmass sample (W2.2) yielded an inverse isochron age of 25.44 ± 0.73 Ma ($P = 0.28$), including 74% of ^{39}Ar released, and is considered robust. One additional sample (G17) produced a *c.* 70% plateau age of 17.0 ± 1.0 Ma, but the clear asymmetrical double-deck shape of the age spectrum and the weathered state of the sample render this age questionable.

Three samples yielded mini-plateau ages ranging from 22.55 ± 0.89 Ma to 28.0 ± 0.81 Ma ($P = 0.23–0.97$). Similar to sample G17, the mini-plateau age spectra show asymmetrical double-deck plateaux and are less reliable than the full plateau ages. Three groundmass samples and one plagioclase sample failed to generate any plateau age.

Major- and trace-element geochemistry of the Ogaden Dyke Swarm lavas

Major- and trace-element geochemical analyses were conducted on all the samples used for dating (or on similar samples collected at the same site), as well as several additional samples (Table 3). All the samples have aphanitic textures showing little visible alteration, except for visible secondary carbonates in samples G5, G7, and G16.

The 20 samples analysed display loss of ignition lower than 1.7 wt% (with the exception of G5, G7 and G16: 2.6–3.5 wt%), testifying to their relative freshness. With the exception of sample MQR9 (51.80 wt% silica), the basalts have relatively low silica content (48.25 ± 2 wt%) and moderate alkali content (3 ± 0.2 wt%) and K_2O/TiO_2 ratios (0.17 ± 0.04 wt%), all typical of transitional

Table 1. *Data on the collected samples and summary of some results*

Sample	Latitude*	Longitude*	Description	$^{40}Ar/^{39}Ar$ (Ma)†	Group	ODS‡
Northern Marda volcanic line						
MA03	9°21′52.13″N	42°41′57.74″E	Basaltic sill, Marda Pass	**23.68 ± 0.54**	2	•
MQR5	9°21′48.73″N	42°42′8.11″E	Shallow intrusion, Marda quarry		2	•
MQR6/7§	9°21′48.51″N	42°42′7.68″E	Dyke, Marda quarry	**25.04 ± 0.65**	2	•
MQR8	9°21′46.11″N	42°42′20.16″E	Shallow intrusion, Marda quarry	22.55 ± 0.89	2	•
MQR9	9°21′15.76″N	42°42′29.51″E	Main Marda basaltic flow, quarry	(discarded)‖	2	○
Eastern Ogaden						
04	6°21′36.64″N	45°56′38.74″E	Lava flow next to dyke, E Raqo Hills	**26.56 ± 0.45**	2	•
11B	6°25′26.97″N	45°50′8.16″E	Lava flow next to dyke, W Raqo Hills	24.40 ± 0.73	2	•
41	6°55′13.84″N	45°12′40.77″E	Ubetale Dyke, SW Werder	(discarded)	1	•
42	6°22′56.49″N	45°30′19.68″E	Lava flow, Ilbah Hills		1	•
G5/7/16§	6°56′25″N	45°47′44″E	Lava flow, Gumburo	(discarded)	1	•
W1.1/4§	6°23′57″N	45°49′18″E	Lava flow, W Raqo Hills	**24.85 ± 0.46**	2	•
W2.1/2/3/8§	6°24′35″N	45°38′3.26″E	Lava flow, Eldibe Hills	**25.44 ± 0.73**	2	•
W3.2/4/7§	6°23′3″N	45°30′12″E	Lava flow, Ilbah Hills	**30.0 ± 1.9**	2	•
Southern Ogaden						
20	5°32′22.12″N	44°35′37.80″E	Mustahil lava flow	28.09 ± 0.81	1	•
WS1.1/2/3§	6°1′10″N	43°21′56″E	Wabe Shebele lava flow, Gode	**7.46 ± 0.47, 6.1 ± 2.4**	2	**X**

*The datum used for the coordinates is WGS84. Geochemical groups are as on Figure 8 and are discussed in the text.
†The ages in bold are defined by robust plateaux or isochrons: the others are from mini-plateaux and therefore questionable, although they are expected to provide a fairly good age range.
‡ODS is marked • when belonging to the Ogaden Dyke Swarm is ascertained by a combination of field, aeromagnetic, and geochemical data, ○ when definitive evidence is lacking, and X when the flow is thought not to be connected with the Ogaden Dyke Swarm.
§Sample names that include '/' represent multiple samples collected at the same site.
‖Two K/Ar ages were obtained by Teledyne Isotopes for Maxus (1993) on the same flow or series of flows: 24.2 ± 1.3 and 25.5 ± 1.3 Ma.

Table 2. *Summary of $^{40}Ar/^{39}Ar$ age data*

Sample ID	Rock type	Material	Plateau characteristics*					Isochron characteristics*			
			Plateau / Mini-plateau age (Ma $\pm 2\sigma$)	Total ^{39}Ar released (%)	Attribute†	MSWD	P	Isochron age (Ma $\pm 2\sigma$)	n	$^{40}Ar/^{36}Ar$ intercept ($\pm 2\sigma$)	MSWD
11	Dyke or flow	Groundmass	24.40 ± 0.73	61	Mini-Pl	0.14	0.97	24.6 ± 1.5	5	291 ± 37	0.17
G17	Flow	Groundmass	16.98 ± 1.0	71	Pl	1.70	0.14	17.2 ± 1.5	6	287 ± 36	2.0
W3.4	Flow	Groundmass	–	–	–	–	–	–	–	–	–
W1.1	Flow	Groundmass	**24.85 ± 0.46**	100	Pl	0.32	0.98	25.13 ± 0.8	11	287 ± 21	0.29
20	Flow	Groundmass	28.09 ± 0.81	64	Mini-Pl	1.4	0.23	28.97 ± 1.5	5	245 ± 62	1.90
MA03	Sill	Groundmass	**23.68 ± 0.54**	100	Pl	1.0	0.44	23.7 ± 2.6	15	299 ± 127	1.1
04	Dyke or flow	Groundmass	**26.56 ± 0.45**	100	Pl	0.92	0.51	26.6 ± 0.5	11	295 ± 7	1.0
41	Dyke	Groundmass	–	–	–	–	–	–	–	–	–
MQR7	Dyke	Groundmass	**25.04 ± 0.65**	100	Pl	0.54	0.91	24.7 ± 1.2	15	305 ± 15	0.51
MQR8	Subsurface intrusive	Groundmass	22.55 ± 0.89	63	Mini-Pl	0.30	0.97	22.5 ± 1.2	9	300 ± 16	0.34
MQR9	Columnar flow	Groundmass	–	–	–	–	–	–	–	–	–
W2.2‡	DF§	Groundmass	24.84 ± 0.57	69	Mini-Pl	2.0	0.06	**25.44 ± 0.73**	9	285 ± 9	1.2
W1.1	Flow	Plagioclase	–	–	–	–	–	–	–	–	–
WS1.1	Flow	Groundmass	**7.46 ± 0.47**	91	Pl	1.30	0.22	7.3 ± 1.5	11	302 ± 35	1.4
WS1.3	Flow	Plagioclase	**6.10 ± 2.4**	92	Pl	0.71	0.65	–	–	–	–
W3.4	Flow	Plagioclase	**30.0 ± 1.9**	83	Pl	0.67	0.72	29.9 ± 2.4	9	298 ± 37	0.79

*Robust plateau and isochron (preferred) ages are indicated in bold and are calculated after Renne *et al.* (2010).
†Pl: plateau; Mini-Pl: mini-plateau; MSWD: Mean square weighted deviation; P: probability value.
‡The inverse isochron age is preferred for sample W2.2 and includes 74% of the ^{39}Ar released.
§No chilled margin was observed but a structural trend in the basalts exists at the surface at this place and is located above a magnetic anomaly.

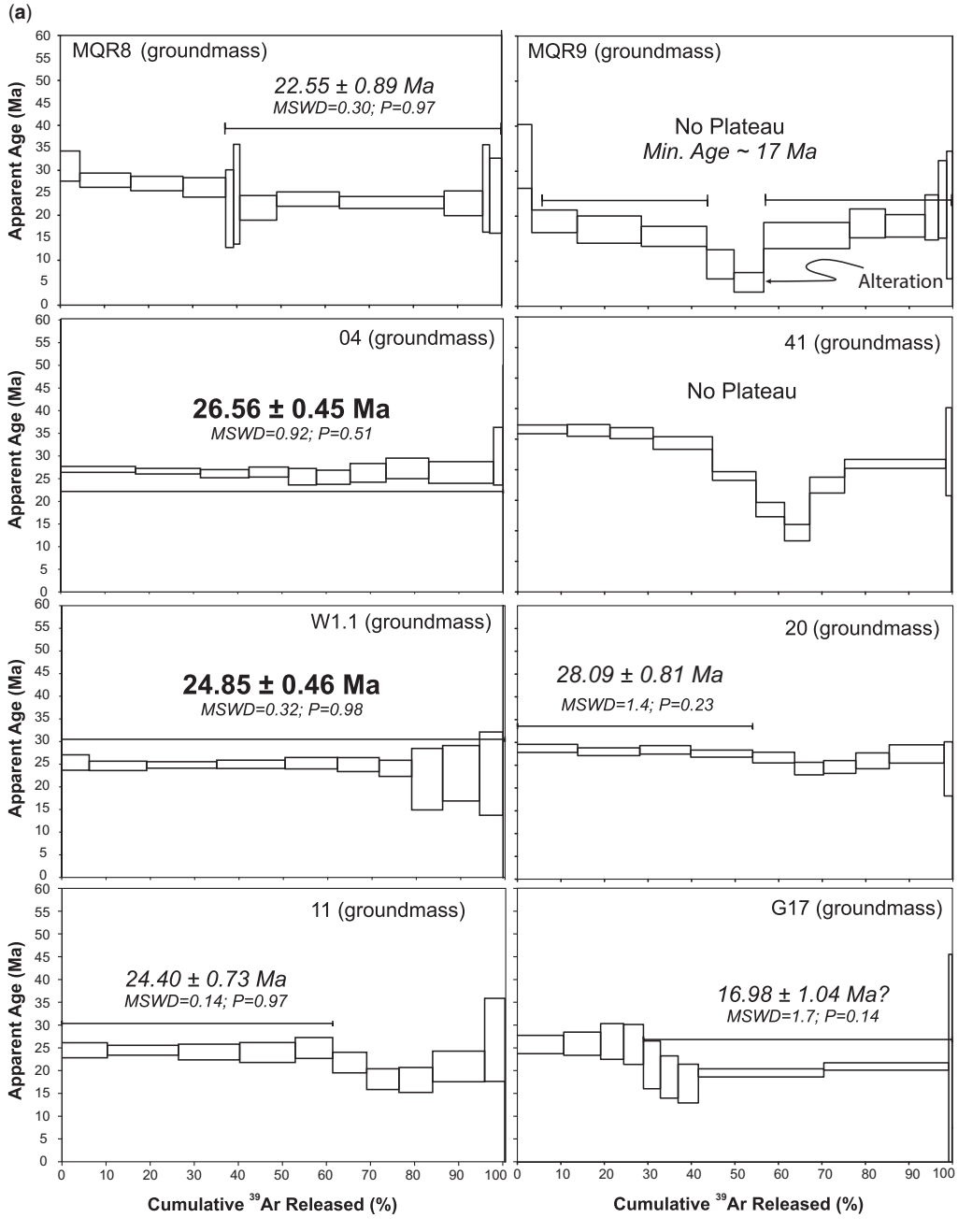

Fig. 7. $^{40}Ar/^{39}Ar$ age spectra and inverse isochron obtained from basalt samples from the Marda Range area and southeastern Ogaden: (**a**) groundmass analyses; (**b**) plagioclase analyses.

tholeiites generated by intra-plate volcanism. The MgO content is, on average, relatively low (*c.* 5.65 $\pm$ 0.2 wt%), suggesting substantial fractionation crystallization prior to eruption. The variations in major elements are too scattered to allow a clear quantification of fractional crystallization processes, but it is clear, nevertheless, that the mineralogical assembly that has fractionated in the

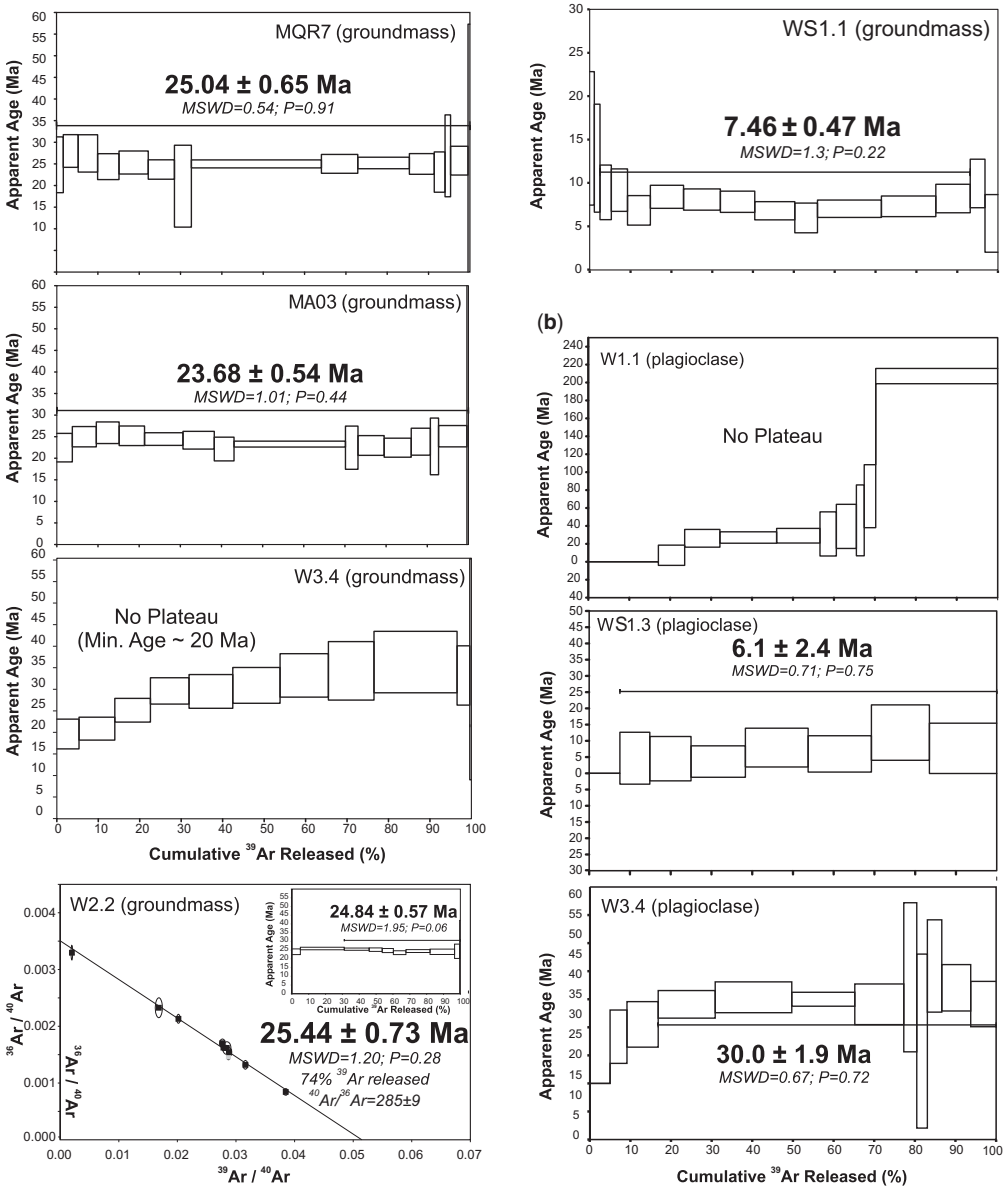

Fig. 7. *Continued.*

magmas is probably composed of plagioclase, clinopyroxene and oxides with or without olivine. We note also the presence of xenocrysts, inherited from the continental crust, of quartz showing disequilibrium features such as corroded contours and coronae of pyroxenes.

The rare earth element (REE) abundances, normalized to chondrite CI (Anders & Grevesse 1989), are presented in Figure 8a. The data indicate strong overall enrichments in light REE relative to middle and heavy REE, with a relatively homogeneous (5% of relative variation) average $(La/Sm)_N$ ratio of *c.* 1.73 $\pm$ 0.09 (N denotes CI chondrite normalization). Conversely, ratios of middle to heavy REEs such as $(Sm/Yb)_N$ display higher variability (14% relative), with an average $(Sm/Yb)_N$ ratio of *c.* 2.69 $\pm$ 0.36. A two-fold subdivision can be made on the basis of these

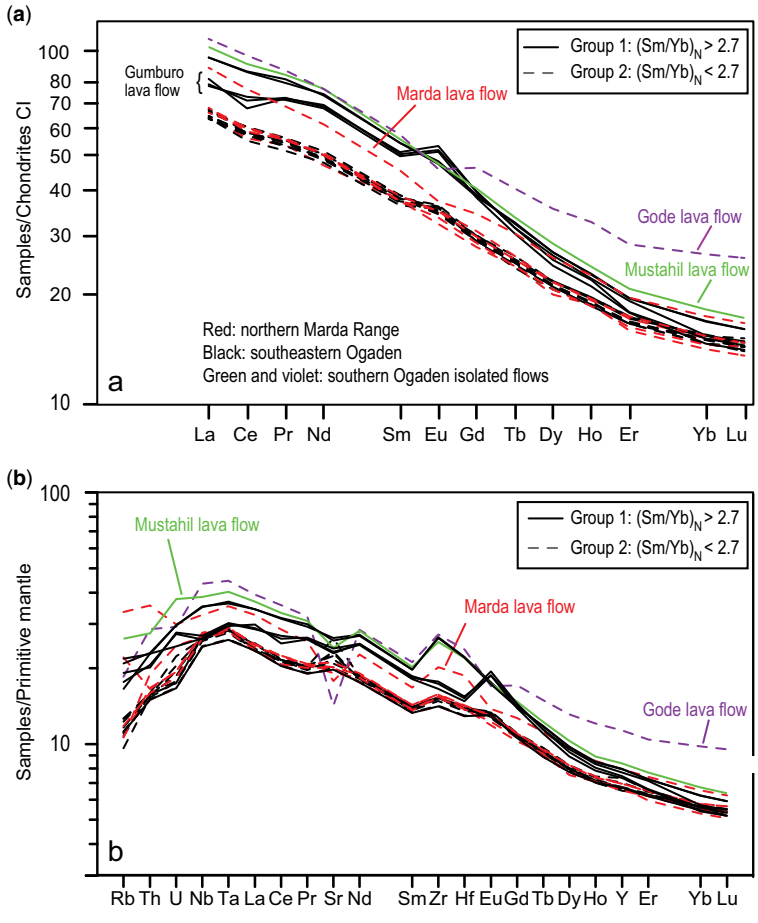

Fig. 8. (**a**) Rare earth element (REE) patterns normalized to CI Chondrites (Anders & Grevesse 1989). (**b**) Extended REE patterns normalized to primitive mantle values (McDonough & Sun 1995). Dashed lines denote samples with $(Sm/Yb)_N < 2.7$; solid lines denote samples with $(Sm/Yb)_N > 2.7$.

ratios: Group 1 (6 samples) is characterized by $(Sm/Yb)_N > 2.7$; and Group 2 (14 samples) by $(Sm/Yb)_N < 2.7$. These REE variations result in non-parallel patterns on Figure 8a, suggesting multiple parental liquids. The extended trace element patterns (Fig. 8a), normalized to the primitive mantle values (McDonough & Sun 1995), show maximum enrichments for Nb and Ta (20–40 times the primitive mantle values) and decreasing enrichments with increasing incompatibility from U to Th and Rb. Highly incompatible trace element ratios indicate small but significant heterogeneity. In Group 1, the Marda lava flow (Sample MQR9) is unusual because of its particularly elevated Rb/Sr (0.057 v. 0.021 ± 0.007), Th/Nb (0.144 v. 0.084 ± 0.009) and Th/La (0.134 vs 0.084 ± 0.006) ratios. This trace element signature, together with a high silica content, might result from significant assimilation of continental crust material. This sample aside, Group 1 shows average lower Rb/Sr (0.019 ± 0.008) and Th/Nb (0.079 ± 0.005) ratios than Group 2 (respectively, 0.025 ± 0.004 and 0.094 ± 0.007). Such differences are subtle but may nevertheless result from slightly different source compositions.

Dyke-swarm characterization

Age and duration of dyke-swarm emplacement

Five plateau and inverse isochron ages constrain the emplacement age of the Ogaden Dyke Swarm to the range 23.7 ± 0.5 to 26.6 ± 0.5 Ma. Based on the age difference between these two end members

and the respective range of uncertainty, we estimate the duration of emplacement as between 2 and 4 myr. An additional plateau age of 30.0 ± 1.9 Ma, obtained on plagioclase separates from a basaltic lava flow, might suggest a longer emplacement period but the disturbed age spectrum from this sample calls into question the reliability of this age determination.

The duration of emplacement of dyke swarms associated with flood basalts is usually of the order of 1–3 myr, regardless of the age of the dykes, as evidenced by the Proterozoic Mackenzie giant dyke swarm (1–2 myr; LeCheminant & Heaman 1989), the Mesozoic Okavango dyke swarm (2 myr; Jourdan *et al.* 2004) and the Miocene dyke swarm of the northern Nevada rift (3 myr or less; Zoback *et al.* 1994). The duration of emplacement of the Ogaden Dyke Swarm emplacement is comparable, albeit at the upper end of the range.

Identification of the erupted products

The geochemical data indicate that most of the sampled lavas were erupted from multiple parental magmas, which were generated, to the first order, from two different sources. Geochemical Group 1 includes all the samples collected at the Marda Pass area (Fig. 3), plus some of the lavas flows identified in the southeastern Ogaden, and two samples next to the dyke at Raqo Hills (samples 4 and 11). The Group 2 lavas are all located in the southeastern Ogaden (Fig. 3). There is no apparent correlation between the chemical compositions, eruption ages, and geographical distribution of the magmas. For instance, the samples 42 and W3.x have different $(Sm/Yb)_N$ ratios but were collected on different sides of the same volcanic hill.

Interestingly, the thick columnar basalt unit capping the Marda Range at the Marda Pass (sample MQR9) is atypical in that it is not derived from the same parental magma as the nearby, stratigraphically lower dykes, and shows unusual assimilation of continental crust. This suggests that the lava flows that formed this capping unit atop the Marda Range were not fed by the Ogaden Dyke Swarm and could have originated further north at, for example, an eruptive centre now located in Afar or beyond.

Several other aspects of the results should be noted.

(1) The Gumburo volcanics crop out only locally in the Gumburo Hills but are seen on the magnetic data to be located above a subsurface dyke and part of an extensive buried lava flow over 90 km long (3 on Fig. 6d). They lie on the Eocene Auradu Formation, and are underlain in the Gumburo-1 well by an aphanitic basaltic sill at 79–122 m and doleritic gabbro at 522–670 m (Straub 1958).

(2) The lavas that formed the Mustahil lava flow in the southern Ogaden (sample 20) have REE patterns similar to those from some lavas erupted from the Ogaden Dyke Swarm. Given the distance of over 140 km between this long sinuous flow and the dyke swarm, it is clear that the dyke-swarm-fed lava flows extended far beyond the known dyke-swarm area. A similar situation has long been recognized in northwestern Ethiopia, where potential feeder dykes for the lava flows along the Blue Nile Gorge are located a minimum of 100 km away (Mohr 1971).

(3) Whilst it had been expected that the similarity in outcrop geomorphology of the Mustahil and Gode lava flows would be reflected in similarities in their geochemistry and age, neither is the case. Where the Mustahil lava flow appears to be closely related to the Ogaden Dyke Swarm history, the Gode lava flow appears totally unrelated. The two $^{40}Ar/^{39}Ar$ plateau ages of 6.1 ± 2.4 Ma and 7.46 ± 0.47 Ma suggest that the Gode lava flow may be related to the much more recent volcanism known along the eastern MER margin, such as in the Ghinir region (Tefera *et al.* 1996). Further work on these younger flows in the western Ogaden is in progress.

Dyke dilation and rifting

The emplacement of the Ogaden Dyke Swarm testifies to the NE–SW-directed tensional forces and dilation in the northern region of what is now the Somalia Plate at the end of the Oligocene and needs to be understood in this regional context.

Basaltic dykes in the Ethiopian LIP seem to be only occasionally emergent, as illustrated by the absence of dykes along the whole Blue Nile Gorge (Mohr 1971), probably because of their negative buoyancy in the uppermost part of the crust (e.g. Lister & Kerr 1991). It can be reasonably suggested that, similar to other flood lava provinces such as the Columbia River Basalt Province, local vent systems may have fed voluminous flows for years, eventually spreading over vast surface areas (Reidel & Tolan 1992; Thordarson & Self 1998; Petcovic & Grunder 2003; Vye-Brown *et al.* 2013). In general, identification of the length and distribution of the erupting segments of the dyke swarm come from indirect evidence; either the dyke swarm is too old and the evidence from the palaeosurface is lacking, or the volcanic province is too young and most of the swarm is not observed. The Ogaden Dyke Swarm is a rare exception in that regard:

lavas erupted from dykes in the southeastern Ogaden are observed (Figs 4c, d & 5a), and the swarm's geomorphological expression, as well as the aeromagnetic data, indicates that it was mainly not emergent.

The dyke dilation must have been accompanied by more or less equivalent tectonic stretching at the surface, as observed for example, in Iceland (e.g. Forslund & Gudmundsson 1991). Curiously, however, there does not appear to be any significant rift structure associated with the Ogaden dyking. Shallow, dyke-related normal faulting may have contributed to the formation of the linear surface depressions, as observed elsewhere (e.g. Wright *et al.* 2006 in Afar; Wall *et al.* 2009 in the North Sea), but the scale is negligible compared to other continental rifts that developed contemporaneously elsewhere in the northern Somali Plate. The largest of these rifts, the Nogal Rift, is parallel to the Ogaden Dyke Swarm and is located approximately 300 km to the NE (Fig. 1). It is revealed by surface outcrops, as well as seismic and drilling data, to be 200 km long and about 35–70 km wide and to contain about 1500 m of syn-rift sediments of Oligo-Miocene age, based on palynology, with no coeval sediments on the rift shoulders (Granath 2001). Reconstructed sections based on seismic reflection profiles suggest about 3.5 km of extension across the Nogal Rift. The Darror Rift, a prominent NNE-trending graben beneath the Darror Valley about 250 km NE of the Nogal Rift, although poorly defined in the subsurface, is known to contain a thick succession of Oligo-Miocene syn-rift sediments (Fantozzi & Sgavetti 1998; Watchorn *et al.* 1998) and is further demonstration of NE–SW extension in the Horn of Africa lithosphere at this time. Other major rift basins of similar age in NE Somalia include the Berbera and Gardafui rift basins (Fantozzi & Sgavetti 1998; Fantozzi & Ali Kassim 2002; Leroy *et al.* 2012).

It is possible that dyke dilation at the Ogaden Dyke Swarm was accommodating at depth part of the coeval tectonic stretching in the Somalia graben in the shallower crust. This offsetting of the dyke dilation and the coeval tectonic stretching has a nearby analogue in the 2 myr-old Sagatu Dyke Swarm (S on Fig. 1), located on and parallel to the eastern margin of the MER (Mohr & Potter 1976; Kennan *et al.* 1990). A similar offset of rift structure and magmatism has been reported for rifts that proceed to oceanization, such as the North Atlantic volcanic margin in East Greenland (e.g. Lenoir *et al.* 2003; Geoffroy 2005).

Accepting that the Red Sea rift basin formed 'very rapidly, analogous to a large, propagating crack' (Bosworth *et al.* 2005, p. 357), we suggest that the intruding plume-derived magma, when it reached the proto-Afar area, was trapped and channelled (as envisaged by Ebinger & Sleep 1998) along the Precambrian shear zone (Shackleton 1996) of the Marda Fault Zone. Normal faulting occurred along the eastern side of the Marda zone in the north. Here, the dykes, or some of them, followed the orientation of the crustal fabric along the northern Marda Fault Zone at N135°E–N140°E, slightly oblique to the maximum horizontal stress (Ziv *et al.* 2000; Schultz *et al.* 2008), similar to other dyke swarms that closely follow the Precambrian fabric (Mège & Korme 2004*a*; Jourdan *et al.* 2006). South of about 8°N, where the Marda Fault Zone appears to splay, the dyke system has followed the eastern splay, which has an orientation of approximately N120°E, co-incidentally the ambient minimum principal stress trajectory imposed by the kinematics of the plate boundaries, that is, parallel to Gulf of Aden spreading axis and the Urumieh-Dokhtar subduction zone.

The Ogaden Dyke Swarm in the geodynamics of the Afar triple junction

Magma source

Over the past two decades, many geochemical studies have highlighted the evolution of the Afar magmatism (Chazot & Bertrand 1993; Zumbo *et al.* 1995; Baker *et al.* 1996*a*, *b*, 1998, 2000; Barrat *et al.* 1998, 2003; Pik *et al.* 1998, 1999; George & Rogers 2002; Bertrand *et al.* 2003; Ukstins Peate *et al.* 2005; Beccaluva *et al.* 2009; Moufti *et al.* 2012; Rooney *et al.* 2013). The contributing geochemical reservoirs have been recognized to be Afar plume material, depleted asthenospheric mantle and Pan-African lithosphere (Marty *et al.* 1996; Furman *et al.* 2006; Rooney *et al.* 2012, 2013 and references therein). Variations in the mixing proportions of the latter components over time have determined a complex evolution of the major elements, trace elements and isotopic compositions in the lavas from this magmatic province. The geochemical evolution can be viewed in the context of Afar lavas, which have evolved over three distinct periods – the Oligocene–Miocene, the Miocene–Pliocene and the Quaternary – and it is useful to view the Ogaden samples in this context.

Figure 9 presents a representative compilation of geochemical data illustrating the evolution of volcanism in the Afar triple junction. The elements are all high field strength elements (HFSE) that are not sensitive to alteration and their ratios should reflect those of corresponding unaltered rocks. Among the elements used, Nb is the most incompatible element and Y the least. The use of incompatible to least-incompatible ratios allows comparison of the relative levels of enrichment of

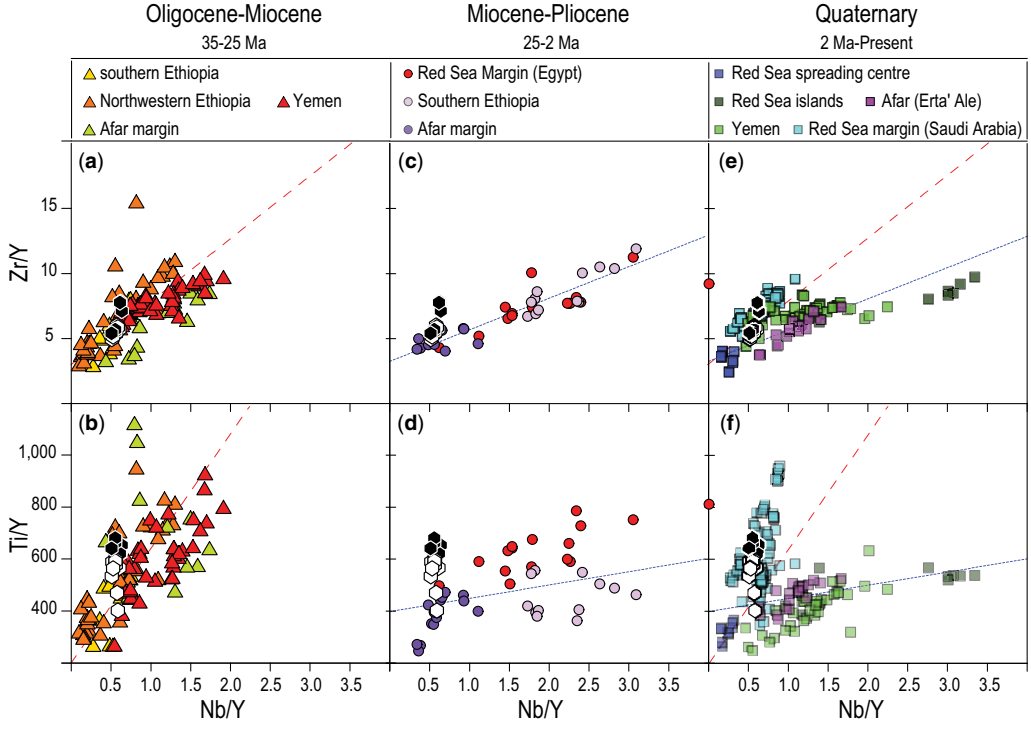

Fig. 9. Plot of Zr/Y and Ti/Y v. Nb/Y for Ogaden samples (white hexagons: low $(Sm/Yb)_N$ samples; black hexagons: high $(Sm/Yb)_N$ samples), compared to the same data for other basalt samples from the Horn of Africa. (**a**, **b**) Oligocene–Miocene samples (yellow triangles, George & Rogers (2002); orange triangles, Pik *et al.* (1998, 1999); red triangle, Baker *et al.* (1996*b*); green triangles, Rooney *et al.* (2013)). (**c**, **d**) Miocene–Pliocene samples (dark purple dot, Rooney *et al.* (2013); pale purple dots, George & Rogers (2002); red dots, Moghazi (2003)). (**e**, **f**) Quaternary samples (dark blue squares, Haase *et al.* (2000); light blue squares, Moufti *et al.* (2012); purple squares, Barrat *et al.* (1998); dark green squares, Volker *et al.* (1997); light green squares, Baker *et al.* (1997)). Samples with MgO < 4 wt% were excluded to screen the data for Fe–Ti oxides that would fractionate the Ti/Y ratio. The red dashed line and blue dotted lines are explained and discussed in the text.

the magmas and their respective sources, assuming that HFSE fractionation during partial melting is more or less the same for all samples. Figure 9a, b presents the chemical variations observed in Oligocene–Miocene lavas. The red dashed line defines a continuous compositional array between depleted samples characterized by low Zr/Y, Ti/Y and Nb/Y ratios, and enriched plume-like samples having high Zr/Y, Ti/Y and Nb/Y ratios. The Ogaden samples, which display little variation on these diagrams, plot on the depleted end (Nb/Y $\sim$ 0.6) of these correlations. Figure 9c, d illustrates the change in chemical composition in the Miocene–Pliocene lavas compared to the Oligocene–Miocene lavas. The blue dotted line defines a trend that shows, for a given Nb/Y ratio, lower Zr/Y and Ti/Y ratios than observed in the Oligocene–Miocene lavas. Most of the Ogaden samples have Ti/Y ratios that are above this trend, too high to be compatible with the chemical systematics defined by Miocene–Pliocene lavas. Finally, the chemical compositions of Quaternary lavas (Fig. 9e, f) plot on both Oligocene–Miocene and Miocene–Pliocene trends. In summary, Figure 9 clearly shows that the Ogaden lavas display geochemical affinities with other Oligocene–Miocene lavas.

A closer comparison of Ogaden samples with Oligocene trap lavas (Fig. 10) indicates that the Ogaden basalts plot within the field defined by high titanium type-1 group of samples (HT1) from the northern Ethiopian plateau (Pik *et al.* 1998, 1999). Previous geochemical and petrological studies (Pik *et al.* 1998, 1999) have shown that those late HT1 lavas originate from the mixing of the Afar plume source – best sampled by high-titanium type-2 (HT2) lavas – and the depleted source seen in low-titanium (LT) lavas. Contamination by continental crustal material also appears to be particularly critical for the most depleted LT samples (Pik *et al.* 1998). The black star in

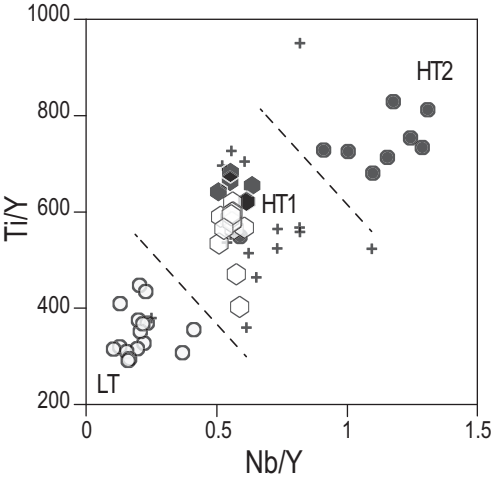

Fig. 10. Plot of Ti/Y v. Nb/Y for Ogaden basalts and northwestern Ethiopian Plateau flood basalts (Pik *et al.* 1998). White hexagons, low $(Sm/Yb)_N$ Ogaden samples; black hexagons, high $(Sm/Yb)_N$ Ogaden samples; white circles, low titanium samples (LT); crosses, high titanium samples type 1 (HT); black dots, high titanium samples type 2 (HT2).

Figure 10 illustrates the composition of the bulk continental crust (Hawkesworth & Kemp 2006). If assimilation of crustal material explains the scatter of Ogaden samples toward low Ti/Y values in Figure 10, its effect is probably negligible in comparison to the overall chemical variations observed in Figure 10. Assuming that the affinity of Ogaden lavas to the HT1 magmas is pertinent, this would imply that the same plume and depleted components are also present in the source of Ogaden samples.

The Ogaden Dyke Swarm has two remarkable peculiarities. Firstly, its emplacement after the main flood lava outpouring event is unusual: dyke swarms in LIPs are characteristically the main source of the flood lava, as they are elsewhere in the Ethiopian volcanic province (Mège *et al.* 2010*a*). Secondly, although coeval with the early dyking along the Red Sea, the Ogaden Dyke Swarm is also distinguished from the Red Sea dykes by a different chemical signature (Fig. 9b) with the composition of the Ogaden dykes reflecting the magmas generated at the Afar plume head.

Evolution of the Afar triple junction: an updated scenario

Our studies show that Tertiary volcanism in SE Ethiopia and adjacent areas of Somalia was far more widespread than previously recognized and is an important element in the pattern of initial rifting in the Afar triple junction. The Ogaden Dyke Swarm occurs in an area historically considered remote from the impact of the Afro-Arabian rifting and volcanism, but it clearly defines a major zone of lithospheric extension along the Red Sea trend across the Horn of Africa. The timing of injection of the Ogaden dykes was contemporaneous with the extensive dyke swarms along the southern Red Sea rift at *c.* 30–21 Ma (Sebai *et al.* 1991; Zumbo *et al.* 1995; Kenea *et al.* 2001). This magmatism occurs, in part at least, along the Marda Fault Zone, commonly thought to be the controlling lithospheric line of weakness along which the Erta 'Ale rift segment developed (Boccaletti *et al.* 1991; Shackleton 1996).

The Ogaden Dyke Swarm can be interpreted as the third 'arm' of an asymmetric Afar triple junction in its embryonic stages 27–24 myr ago. The Nogal and other contemporaneous rift basins of northeastern Somalia are further evidence of the NE–SE-directed tensional forces acting on the Horn of Africa at that time.

The following tectonic scenario, shown schematically on Figure 11, accommodates our recent findings and the published information.

(1) At 31–28 Ma (Hofmann *et al.* 1997), mantle plume-related volcanism caused eruption of the Ethiopian flood basalts contemporaneous with subduction of the Neotethys Ocean along the Urumieh-Dokhtar subduction zone (McQuarrie *et al.* 2003) (Fig. 11a). Between 30 Ma and 27.5 Ma, rifting started in the southern Red Sea and western Gulf of Aden (Hughes *et al.* 1991) in response to slab pull on the weakened Afar lithosphere (Fig. 11b).

(2) Rifting continued from 27 Ma to 21 Ma, still driven by the Urumieh-Dokhtar subduction, with rift basins forming in Yemen and Somalia (e.g. Leroy *et al.* 2012) and emplacement of the Ogaden Dyke Swarm parallel to the rift basins. Extension is predominantly ENE directed at this time – the Somalia Plate had not begun to rotate away from Africa – and the Afar triple junction is an asymmetrical rupture with the Ogaden and Red Sea arms sub-parallel. The Ogaden Dyke Swarm, dated 27–24 Ma, can be considered as the third arm of the Afar triple junction during this period. It is coeval with the Radfan dyke swarm in Yemen and of similar orientation (Moseley 1969; Zumbo 1995). Tectonic and magmatic activity of similar age occurred along the western margin of Afar with a similar NNW–SSE structural orientation (Zanettin & Justin-Visentin 1975; Wolfenden *et al.* 2005). There is, therefore, remarkably continuous dyking and extensional tectonic activity from the Red Sea to eastern Ogaden at

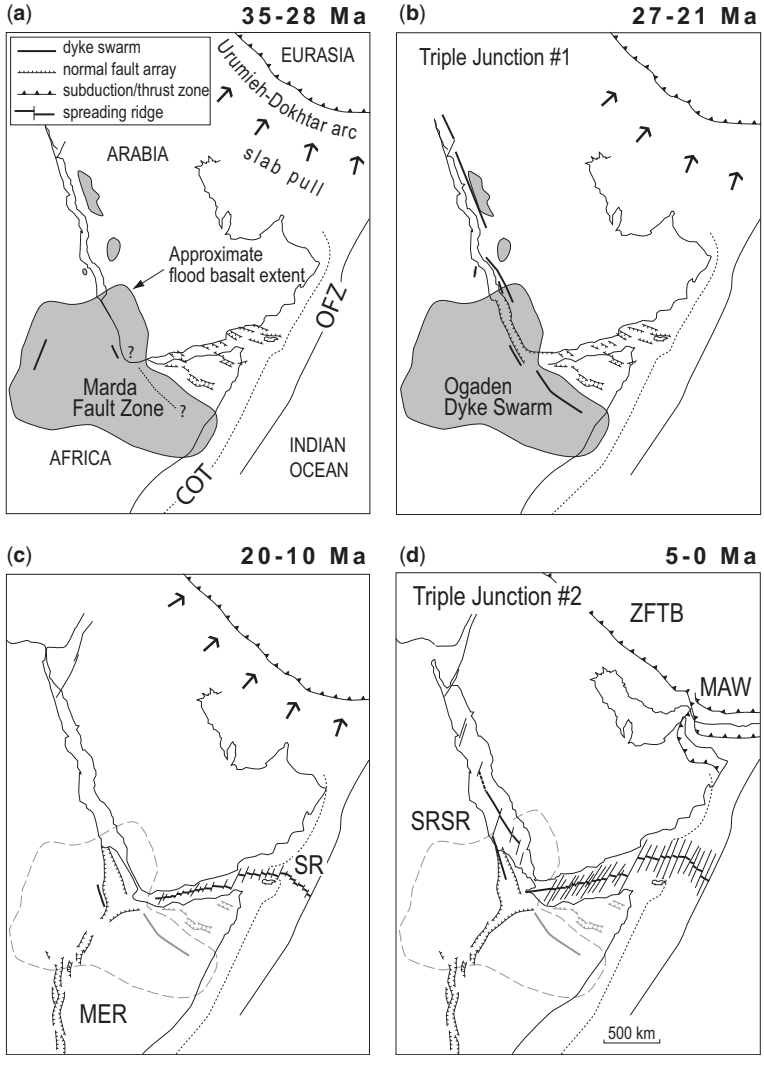

Fig. 11. Schematic reconstruction of the evolution of the Afar triple junction. The base maps are modified from Bosworth *et al.* (2005). Flood basalt extent is approximate and based on the location of the outcrops described in the literature and, in eastern Ethiopia and Somalia, on geological mapping by the authors, oil- and water-well data (Faillace 1993), and vintage Esso and Elf aeromagnetic surveys (Bosellini 1989). The exact extent of the Marda Fault Zone outside its outcrop area (**a**, **b**) is not constrained. COT, continent–ocean transition; MAW, Makran Accretionary Wedge; MER, Main Ethiopian Rift; OFZ, Owen Fracture Zone; SR, Sheba Ridge; SRSR, Southern Red Sea Ridge; ZFTB, Zagros Fold-and-Thrust Belt. The inactive tectonic patterns are grey coloured on (**c**) and (**d**).

that time, via what is now the western Afar. Dyke-swarm emplacement continued along the southern Red Sea until 21 Ma (Sebai *et al.* 1991; Zumbo *et al.* 1995) and the northern Red Sea Rift propagated to the Mediterranean (Bosworth *et al.* 2005). Rifting occurred at this time in the Turkana/Omo region (Davidson 1983) and to the north near Jemma (Wolela 2004), and possibly in the intervening region (see locations on Fig. 1). The chemical composition of the Ogaden Dyke Swarm is typical of the Afar plume, well after the main flood basalt eruption peak.

(3) At *c.* 20 Ma, the East African Rift system was reoriented, and rifting commenced in the Chamo and Galana graben (location on Fig. 1) of the southern MER (Ebinger *et al.* 1993). Contemporaneously, oceanic spreading

Table 3. *Major and trace element results for Ogaden samples and georeferenced material used in the external calibration*

Sample	MQR8	MQR5	MQR6	MQR9	MA03	11B	42	4	20	41	W1.4	W2.8	W2.1	W2.3	W3.7	W3.2	WS1.2	G16	G5	G7
Rock type	Basalt	Basalt	Basalt	Basalt	Basalt	Basalt	Basalt	Basalt	Basalt	Basalt	Basalt	Basalt	Basalt	Basalt	Basalt	Basalt	Basalt	Basalt	Basalt	Basalt
SiO_2 (wt%)	51.03	48.10	47.86	51.80	47.67	47.65	48.59	47.43	48.63	48.40	47.37	48.15	47.32	47.58	47.37	47.83	48.54	49.61	47.25	47.48
TiO_2	2.67	2.79	2.86	2.65	2.77	2.87	3.49	2.83	3.91	3.53	2.84	2.78	2.88	2.78	2.76	2.80	3.34	3.38	3.59	3.45
Al_2O_3	14.07	14.56	14.55	13.47	14.39	14.31	14.00	14.41	13.44	14.08	14.38	14.65	14.48	14.44	14.52	15.08	13.11	12.82	13.16	13.02
$Fe_2O_3^T$	12.85	13.78	13.68	12.96	13.60	13.75	14.26	14.18	14.91	14.08	14.05	14.02	13.91	13.88	13.89	14.18	14.63	13.55	13.88	13.78
MnO	0.181	0.195	0.191	0.186	0.190	0.192	0.182	0.200	0.207	0.204	0.198	0.201	0.202	0.190	0.203	0.198	0.211	0.165	0.174	0.178
MgO	5.84	6.27	6.14	5.58	6.16	5.83	4.24	5.91	5.17	5.48	6.21	5.96	5.97	5.86	5.31	4.49	6.44	4.99	4.99	5.42
CaO	9.88	10.52	10.56	9.47	10.37	10.73	9.80	11.39	9.15	9.55	10.84	10.83	10.95	11.13	11.39	11.17	10.23	9.14	9.45	10.04
Na_2O	2.48	2.64	2.64	2.48	2.51	2.59	2.72	2.61	2.78	2.76	2.65	2.61	2.61	2.60	2.62	2.69	2.52	2.23	2.36	2.03
K_2O	0.335	0.496	0.387	0.850	0.378	0.416	0.597	0.487	0.719	0.667	0.476	0.506	0.470	0.493	0.483	0.370	0.473	0.507	0.495	0.545
P_2O_5	0.337	0.370	0.374	0.291	0.355	0.355	0.591	0.351	0.582	0.586	0.356	0.372	0.362	0.354	0.370	0.358	0.571	0.765	0.805	0.795
LOI	0.27	0.35	0.66	0.33	1.21	0.68	1.77	0.80	0.49	0.63	−0.05	0.45	0.73	0.83	1.00	1.73	0.74	2.75	2.62	3.50
Sum	99.95	100.08	99.90	100.06	99.60	99.37	100.24	100.59	99.99	99.96	99.31	100.53	99.88	100.14	99.92	100.88	100.81	99.89	98.77	100.23
Sc (ppm)	30.8	33.0	32.8	35.6	32.0	31.5	29.9	32.1	29.1	29.3	33.5	31.8	31.8	32.7	32.3	32.6	40.6	27.9	28.5	28.2
V	369	394	395	330	386	376	384	373	397	381	406	393	390	394	383	409	451	339	344	346
Cr	97	101	100	20	99	99	62	98	51	62	100	98	98	101	98	103	147	101	103	104
Co	45.6	46.0	47.7	45.2	45.3	45.2	34.0	44.0	41.9	46.1	46.6	47.0	46.3	46.5	48.3	38.4	45.3	37.1	38.1	38.1
Ni	53.6	47.4	50.6	29.6	50.3	51.5	33.8	48.6	28.7	41.8	51.9	52.8	53.1	53.9	51.0	44.3	70.1	57.0	59.0	58.7
Cu	41.3	47.2	46.6	95.2	45.1	42.8	33.7	41.6	37.9	33.9	53.2	46.4	46.5	46.0	45.5	45.9	242.9	45.4	47.1	44.2
Zn	109	116	116	111	127	112	130	107	134	135	117	115	114	115	115	113	126	117	122	119
Rb	6.3	6.3	13.2	20.0	7.0	7.3	13.1	6.7	15.7	12.5	6.4	6.9	5.7	7.6	6.6	7.5	11.1	9.9	11.5	10.6
Sr	379	400	417	352	398	396	525	393	480	512	453	413	430	461	519	443	281	462	477	456
Y	27.9	29.7	29.7	33.9	28.7	28.2	34.2	28.8	36.0	34.3	28.7	28.8	27.9	28.4	31.3	30.0	48.4	31.5	32.1	33.1
Zr	160	165	164	211	161	160	279	148	267	277	160	160	155	158	160	159	284	174	182	186
Nb	17.4	17.9	18.1	21.3	17.2	17.1	23.2	16.0	25.3	23.0	17.5	17.4	16.8	17.0	17.3	17.1	28.4	17.3	17.7	17.1
Cs	0.098	0.062	0.332	0.226	0.178	0.111	0.244	0.097	0.269	0.199	0.087	0.100	0.084	0.120	0.096	0.123	0.100	0.172	0.177	0.224
Ba	197	179	199	211	160	172	401	1362	255	254	949	297	1104	903	1250	450	234	577	809	291
La	16.1	16.0	15.7	21.0	15.2	15.4	22.2	15.2	23.8	22.2	15.1	15.3	15.1	15.1	16.0	16.2	25.3	18.5	18.7	19.3
Ce	37.3	37.3	37.4	47.6	34.6	36.0	52.7	34.2	55.5	53.0	35.8	36.0	35.3	35.6	36.0	36.3	59.3	45.0	43.9	42.0
Pr	5.18	5.23	5.25	6.43	5.06	5.13	7.42	4.83	7.82	7.59	5.08	5.08	4.97	5.00	5.16	5.19	8.11	6.65	6.73	6.62
Nd	22.8	23.4	23.7	28.2	21.8	22.6	34.0	22.0	35.2	33.6	22.5	23.3	22.9	22.4	23.1	23.1	35.4	30.9	31.3	31.3
Sm	5.49	5.77	5.77	6.77	5.57	5.65	8.01	5.40	8.21	8.02	5.65	5.66	5.49	5.55	5.68	5.75	8.55	7.36	7.55	7.44
Eu	1.88	1.98	1.99	2.11	1.82	1.94	2.71	2.01	2.67	2.66	2.04	1.96	2.03	2.02	2.06	1.98	2.60	2.88	2.99	2.88
Gd	5.74	5.95	5.99	6.87	5.54	5.77	7.71	5.76	8.02	7.61	5.86	5.84	5.75	5.77	5.97	5.92	9.26	7.55	7.85	7.84
Tb	0.89	0.94	0.93	1.10	0.90	0.91	1.16	0.88	1.21	1.17	0.92	0.92	0.90	0.91	0.95	0.93	1.47	1.09	1.13	1.13
Dy	5.18	5.49	5.51	6.39	5.04	5.34	6.58	5.22	6.95	6.56	5.35	5.38	5.31	5.31	5.51	5.46	8.78	6.02	6.26	6.43
Ho	1.05	1.09	1.10	1.27	1.05	1.06	1.26	1.05	1.33	1.27	1.07	1.06	1.04	1.04	1.10	1.09	1.79	1.17	1.20	1.24
Er	2.70	2.82	2.84	3.22	2.60	2.74	3.18	2.72	3.38	3.17	2.73	2.76	2.72	2.72	2.85	2.81	4.54	2.89	2.90	3.13
Yb	2.41	2.54	2.53	2.87	2.32	2.48	2.75	2.41	2.97	2.76	2.48	2.46	2.41	2.46	2.52	2.49	4.29	2.38	2.46	2.52
Lu	0.357	0.375	0.375	0.420	0.335	0.359	0.401	0.351	0.427	0.397	0.365	0.363	0.364	0.358	0.370	0.371	0.641	0.346	0.357	0.375
Hf	3.86	4.01	3.98	5.26	3.89	3.89	6.27	3.65	6.21	6.23	3.94	3.93	3.80	3.85	3.91	3.89	6.69	4.19	4.30	4.37
Ta	1.05	1.07	1.07	1.30	1.03	1.04	1.34	0.96	1.49	1.36	1.07	1.05	1.02	1.04	1.05	1.04	1.64	1.11	1.12	1.09
Th	1.50	1.32	1.31	2.81	1.26	1.26	1.81	1.19	2.19	1.83	1.24	1.24	1.21	1.22	1.24	1.26	2.26	1.82	1.60	1.64
U	0.496	0.391	0.392	0.603	0.370	0.358	0.601	0.338	0.765	0.601	0.352	0.377	0.355	0.393	0.413	0.450	0.589	0.496	0.563	0.555
$(Sm/Yb)_N$	2.5	2.4	2.5	2.6	2.6	2.5	3.2	2.4	3.0	3.2	2.5	2.5	2.5	2.5	2.5	2.5	2.2	3.4	3.3	3.2

Major elements in wt% and trace elements in ppm.

commenced in the Gulf of Aden (Fournier *et al.* 2010) (Fig. 11c) along the Sheba Ridge, de-stressing the lithosphere in the northern Somali Plate. We suggest the Marda/Ogaden 'arm' of the initial Afar triple junction atrophied at this time, as rifting and dyke injection ceased. At *c.* 11 Ma rifting began in southern Afar and propagated SW to join the southern MER at *c.* 5 Ma (Bonini *et al.* 2005) when southern Red Sea spreading (Cochran & Karner 2007) commenced in northern Afar along the Erta 'Ale segment.

(4) At *c.* 5 Ma (Bonini *et al.* 2005), the modern Afar triple junction exists with an extent and geometry similar to that of today with three arms *c.* 120° apart (Fig. 11d).

Conclusions

Extensive studies of aerial and satellite imagery, coupled with helicopter-supported and road-based field surveys in 2005–12 have provided a new map of the volcanic outcrops in Ogaden region in SE Ethiopia. Helicopter support allowed us to visit and sample remote outcrops, not otherwise accessible, in the eastern and southern Ogaden and was essential for time-efficient and safe operations in this region where security conditions can be a concern.

The Marda Fault Zone, though still very little understood, is confirmed by this recent work as a fundamental tectonic element of the Horn of Africa. Recently-cut gravel quarries in the basalt outcrops capping the Marda Range near Jijiga have improved our understanding of this feature by revealing massive columnar lava flows and a major dyke system penetrating the Jurassic sediments.

Vintage and modern magnetic data across and east of the Marda Fault Zone, respectively, reveal linear, high amplitude, SSE- to SE-trending anomalies of both normal and reverse polarity interpreted as dykes from at least two periods of injection. The magnetic data also reveal large areas of surface and shallow-level basalts, showing that the scattered outcrops they encompass are not remote unconnected occurrences but parts of extensive volcanic units. Several lava flows were channelled within, and overflowed the banks of, meandering river palaeovalleys, as observed elsewhere in outcrop in the Ogaden. The dyke system cuts through the lava flows and provided the feeder system. Several volcanic hills and mounds, which are co-incident with observed linear magnetic anomalies, are thought to be dyke related, but most have a surface of mainly rounded cobbles and pebbles, and outcrops revealing chilled margins and other defining features are rare. Many of the dykes are overlain by shallow surface depressions thought to be tensional fracturing above the rising dyke tip.

Integration of the magnetic and geological data has revealed a dyke swarm extending from the southern Afar margin over 600 km across the Somali Plate to the Ethiopia–Somalia border. $^{40}Ar/^{39}Ar$ age dating of the outcrops shows that emplacement of the dykes and the associated flows occurred at 27–24 Ma, co-incident with the main dyking event in the southern Red Sea. Geochemical and geochronological analyses show that the dyke intrusions in the Marda Fault Zone and some of the eastern Ogaden are derived from the same parental magma, demonstrating a common source for much of the lava injected in the Ogaden Dyke Swarm and distributed in lava flows as far east as the Ethiopia–Somalia southeastern border. Such close genetic relationships could not be established for the Marda Range extrusives and intrusives.

The Ogaden Dyke Swarm is a zone of crustal dilation continuing the Red Sea trend across the Horn of Africa and needs to be incorporated into tectonic schemes for this region. We speculate that when the Red Sea rift basin rapidly propagated south at *c.* 27 Ma, the plume magma, upon reaching the proto-Afar area, may have been trapped and channelled along the Precambrian Marda shear zone. The dykes of the Ogaden Dyke Swarm propagated in a thick sequence of Phanerozoic sediments and followed the major sub-vertical fabric of the Marda Fault Zone. Given that the MER did not become an arm of the Afar triple junction until *c.* 5 Ma, we suggest that the Ogaden Dyke Swarm might be viewed as the 'original' third arm of the embryonic Afar triple junction. The NE–SW-trending Nogal and Darror Oligo-Miocene rifts are further expressions of the NE–SW-directed lithospheric tension at that time linked to slab pull emanating from the Urumieh-Dokhtar subduction zone.

The volcanic rock outcrops on the rift shoulder SE of the MER and Afar are far more extensive than usually recognized. The work to date suggests that a better understanding of their distribution, age and geochemistry will help in understanding the tectono-magmatic development of this fascinating region. Our future work will focus on mapping and sampling outcrops in the western Ogaden, more detailed mapping, analyses of basalt lava flows and dykes along the Marda Fault Zone, and the correlation of causative tectono-magmatic events with those in the adjacent regions.

References

Abdirahim, M. M., Ali Kassim, M., Carmignani, L. & Coltorti, M. 1993. The geomorphological evolution of the upper Juba valley in southern Somalia.

In: Abbate, E., Sagri, M. & Sassi, F. P. (eds) *Geology and Mineral Resources of Somalia and Surrounding Regions*. Istituto Agronomico per l'Oltremare, Relazioni E Monografie Agrarie Subtropicali e Tropicale, Florence, Italy, **113A**, 241–250.

Anders, E. & Grevesse, N. 1989. Abundances of the elements: meteoritic and solar. *Geochimica et Cosmochimica Acta*, **53**, 197–214.

Audin, L., Quidelleur, X. *et al*. 2004. Paleomagnetism and K-Ar and $^{40}Ar/^{39}Ar$ ages in the Ali Sabieh area (Republic of Djibouti and Ethiopia): constraints on the mechanism of Aden ridge propagation into southeastern Afar during the last 10 My. *Geophysical Journal International*, **158**, 327–345.

Autin, J., Leroy, S. *et al*. 2009. Continental break-up history of a deep magma-poor margin based on seismic reflection data (northeastern Gulf of Aden margin, offshore Oman). *Geophysical Journal International*, **180**, 501–519, http://doi.org/10.1111/j.1365-246X.2009.04424.x

Baer, G. & Hamiel, Y. 2010. Form and growth of an embryonic continental rift: InSAR observations and modelling of the 2009 western Arabia rifting episode. *Geophysical Journal International*, **182**, 155–167, http://doi.org/10.1111/j.1365-246X.2010.04627.x

Baker, G., Chazot, G., Menzies, M. & Thirlwall, M. 1998. Metasomatism of the shallow mantle beneath Yemen by the Afar plume – Implications for mantle plumes, flood volcanism, and intraplate volcanism. *Geology*, **26**, 431–434.

Baker, J. A., Snee, L. & Menzies, M. A. 1996*a*. A brief Oligocene period of flood volcanism in Yemen: implications for the duration and rate of continental flood volcanism at the Afro-Arabian triple junction. *Earth and Planetary Science Letters*, **138**, 39–55.

Baker, J. A., Thirlwall, M. F. & Menzies, M. A. 1996*b*. Sr–Nd–Pb isotopic and trace element evidence for crustal contamination of plume-derived flood basalts: Oligocene flood volcanism in western Yemen. *Geochimica et Cosmochimica Acta*, **60**, 2559–2581.

Baker, J. A., Menzies, M. A., Thirlwall, M. F. & MacPherson, C. G. 1997. Petrogeneis of quaternary intraplate volcanism, Sana'a, Yemen: implications for plume–lithosphere interaction and iolybaric melt hybridization. *Journal of Petrology*, **38**, 1359–1390.

Baker, J. A., MacPherson, C. G., Menzies, M. A., Thirlwall, M. F., Al-Kadasi, M. & Mattey, D. P. 2000. Resolving crustal and mantle contributions to continental flood volcanism, Yemen; Constraints from mineral oxygen isotope data. *Journal of Petrology*, **41**, 1805–1820.

Barrat, J.-A., Fourcade, S., Jahn, M. B., Cheminée, J.-L. & Capdevila, R. 1998. Isotope (Sr, Nd, Pb, O) and trace element geochemistry of volcanism from Erta'Ale range (Ethiopia). *Journal of Volcanology and Geothermal Research*, **80**, 85–100.

Barrat, J.-A., Joron, J.-L., Taylor, R. N., Fourcade, S., Nesbitt, R. W. & Jahn, B. M. 2003. Geochemistry of basalts from Manda Hararo, Ethiopia: LREE-depleted basalts in central Afar. *Lithos*, **69**, 1–13.

Beccaluva, L., Bianchini, G., Natali, C. & Siena, F. 2009. Continental flood basalts and mantle plumes: a case study of the Northern Ethiopian Plateau. *Journal of Petrology*, **50**, 1377–1403.

Bertrand, H., Chazot, G., Blichert-Toft, J. & Thoral, S. 2003. Implications of widespread high-m volcanism on the Arabian Plate for the Afar mantle plume and lithosphere composition. *Chemical Geology*, **198**, 47–61.

Black, R., Morton, W. H. & Tsegaye, H. 1974. Early Structures around the Afar Triple Junction. *Nature*, **248**, 496–497.

Boccaletti, M., Getaneh, A. & Bonavia, F. F. 1991. The Marda fault: a remnant of an incipient aborted rift in the paleo-African Arabian plate. *Journal of Petroleum Geology*, **14**, 79–92.

Bonini, M., Corti, G., Innocenti, F., Manetti, P., Mazzarini, F., Abebe, T. & Pecskay, Z. 2005. Evolution of the Main Ethiopian Rift in the frame of Afar and Kenya rifts propagation. *Tectonics*, **24**, TC1007, http://doi.org/10.1029/2004TC001680

Bosellini, A. 1989. The continental margins of Somalia: their structural evolution and sequence stratigraphy. *Memorie di Scienze Geologiche*, **41**, 373–458.

Bosworth, W., Huchon, P. & McClay, K. 2005. The Red Sea and Gulf of Aden basins. *Journal of African Earth Sciences*, **43**, 334–378, http://doi.org/10.1016/j.jafrearsci.2005.07.020

Bottenberg, H. C. 2012. *Plate Kinematics of the Afro-Arabian Rift System with Emphasis on the Afar Depression, Ethiopia*. PhD thesis, Missouri University of Science and Technology.

Brown, B. 1943. Palaeontology of Harrar Province, Ethiopia. Part 1, The Dudley Expedition. *Bulletin of the American Museum of Natural History*, **82**, 1–30.

Burov, E. & Guillou-Frottier, L. 2005. The plume head-continental lithosphere interaction using a tectonically realistic formulation for the lithosphere. *Geophysical Journal International*, **161**, 469–490.

Chazot, G. & Bertrand, H. 1993. Mantle sources and magma-continental crust interactions during early Red Sea-Aden rifting in Southern Yemen: elemental and Sr, Nd, Pb isotope evidence. *Journal of Geophysical Research*, **98**, 1819–1835.

Chorowicz, J., Collet, B., Bonavia, F. F., Mohr, P., Parrot, J.-F. & Korme, T. 1998. The Tana basin, Ethiopia: intra-plateau uplift, rifting and subsidence. *Tectonophysics*, **295**, 351–367.

Cochran, J. R. & Karner, G. D. 2007. Constraints on the deformation and rupturing of continental lithosphere of the Red Sea: the transition from rifting to drifting. *In*: Karner, G. D., Manatschal, G. & Pinheiro, L. M. (eds) *Imaging, Mapping and Modelling Continental Lithosphere Extension and Breakup*. Geological Society, London, Special Publication, **282**, 265–289, http://doi.org/10.1144/SP282.13

Davidson, A. 1983. *Reconnaissance Geology and Geochemistry of Ilubabor, Keka, Gemu Gofa and Sidamo, Ethiopia*. Ethiopian Institute of Geological Surveys Bulletin, **2**.

Ebinger, C. J. & Sleep, N. 1998. Cenozoic magmatism throughout east Africa resulting from impact of a single plume. *Nature*, **395**, 788–791.

Ebinger, C., Yemane, T., Woldegabriel, G., Aronson, J. L. & Walter, R. C. 1993. Late Eocene–Recent volcanism and faulting in the southern main Ethiopian rift. *Journal of the Geological Society, London*, **150**, 99–108, http://doi.org/10.1144/gsjgs.150.1.0099

EBINGER, C. J., YEMANE, T., HARDING, D. J., TESFAYE, S., KELLEY, S. & REX, D. C. 2000. Rift deflection, migration, and propagation: linkage of the Ethiopian and Eastern rifts, Africa. *Geological Society of America Bulletin*, **112**, 163–176.

FAILLACE, C. 1993. Hydrogeological importance of the sub-surface basalts in the Mudug-Galgadud plateau. *In*: ABBATE, E., SAGRI, M. & SASSI, F. P. (eds) *Geology and Mineral Resources of Somalia and Surrounding Regions, Volume B, Mineral and Water Resources*. Istituto Agronomico per l'Oltremare, Relazione e Monografie, Firenze, Italy, **113**, 649–664.

FANTOZZI, P. L. & ALI KASSIM, M. 2002. Geological mapping in northeastern Somalia (Midjiurtinia region): field evidence of the structural and paleogeographic evolution of the northern margin of the Somalian plate. *Journal of African Earth Sciences*, **34**, 21–55.

FANTOZZI, P. L. & SGAVETTI, M. 1998. Tectonic and sedimentary evolution of the eastern Gulf of Aden continental margins: new structural and stratigraphic data from Somalia and Yemen. *In*: PURSER, B. H. & BOSENCE, D. W. J. (eds) *Sedimentation and Tectonics of Rift Basins: Red Sea–Gulf of Aden*. Chapman and Hall, London, 56–76.

FORSLUND, T. & GUDMUNDSSON, A. 1991. Crustal spreading due to dikes and faults in southwest Iceland. *Journal of Structural Geology*, **13**, 443–457.

FOURNIER, M., CHAMOT-ROOKE, N. *ET AL.* 2010. Arabia-Somalia plate kinematics, evolution of the Aden-Owen-Carlsberg triple junction, and opening of the Gulf of Aden. *Journal of Geophysical Research*, **115**, B04102, http://doi.org/10.1029/2008JB006257

FURMAN, T., BRYCE, J., ROONEY, T., HANAN, B., YIRGU, G. & AYALEW, D. 2006. Heads and tails: 30 million years of the Afar plume. *In*: YIRGU, G., EBINGER, C. J. & MAGUIRE, P. K. H. (eds) *The Afar Volcanic Province within the East African Rift System*. Geological Society, London, Special Publications, **259**, 95–119, http://doi.org/10.1144/GSL.SP.2006.259. 01.09

GARFUNKEL, Z. & BEYTH, M. 2006. Constraints on the structural development of Adar imposed by the kinematics of the major surrounding plates. *In*: YIRGU, G., EBINGER, C. J. & MAGUIRE, P. K. H. (eds) *The Afar Volcanic Province within the East African Rift System*. Geological Society, London, Special Publications, **259**, 23–42, http://doi.org/10.1144/GSL.SP.2006.259.01.04

GEOFFROY, L. 2005. Volcanic passive margins. *Comptes Rendus Geoscience*, **337**, 1395–1408.

GEORGE, R. M. & ROGERS, N. W. 2002. Plume dynamics beneath the African plate inferred from the geochemistry of Tertiary basalts of southern Ethiopia. *Contributions to Mineralogy and Petrology*, **144**, 286–304.

GEOSURVEY 1977. *Harar Aeromagnetic Survey, East Central Ethiopia*. Interpretation and Operations Report for Whitestone Petroleum Company, Ethiopia.

GOUIN, P. & MOHR, P. A. 1964. Gravity traverses in Ethiopia (Interim Report). *Bulletin of the Geophysical Observatory, Addis Ababa*, **3**, 185–239.

GRANATH, J. W. 2001. The Nogal Rift of northern Somalia: Gulf of Aden, reactivation of a Mesozoic rift. *In*: ZIEGLER, P. A., CAVAZZA, W., ROBERTSON, A. H. F. & CRASQUIN-SOLEAU, S. (eds) *Peri-Tethys Memoir 6*. Mémoires du Muséum d'Histoire Naturelle, Paris, **186**, 511–527.

HAASE, K., MÜHE, R. & STOFFERS, P. 2000. Magmatism during extension of the lithosphere: geochemical constraints from lavas of the Shaban Deep, northern Read Sea. *Chemical Geology*, **166**, 225–239.

HALLS, H. & FAHRIG, W. (eds) 1987. *Mafic Dyke Swarms*. Geological Association of Canada Special Papers 34.

HAWKESWORTH, C. J. & KEMP, A. I. S. 2006. Evolution of the continental crust. *Nature*, **443**, 811–817.

HOFMANN, C., COURTILLOT, V., FÉRAUD, G., ROCHETTE, P., YIRGU, G., KETEFO, E. & PIK, R. 1997. Timing of the Ethiopian flood basalt event and implication for plume birth and global change. *Nature*, **389**, 838–841.

HUGHES, G. W., VAROL, O. & BEYDOUN, Z. R. 1991. Evidence for Middle Oligocene rifting of the Gulf of Aden and for Late Oligocene rifting of the southern Red Sea. *Marine and Petroleum Geology*, **8**, 354–358.

JOURDAN, F., FÉRAUD, G. *ET AL.* 2004. The Karoo triple junction questioned: evidence from Jurassic and Proterozoic $^{40}Ar/^{39}Ar$ ages and geochemistry of the giant Okavango dyke swarm (Botswana). *Earth and Planetary Science Letters*, **222**, 989–1006.

JOURDAN, F., FÉRAUD, G. *ET AL.* 2006. Basement control on dyke distribution in large igneous provinces: case study of the Karoo triple junction. *Earth and Planetary Science Letters*, **241**, 307–322.

JUCH, D. 1975. Geology of the southeastern escarpment of Ethiopia between 39° and 42° longitude east. *In*: PILGER, A. & ROSLER, A. (eds) *Proceedings of an International Symposium on the Afar Region and Related Rift Problems, held in Bad Bergzabern, F. R. Germany, April 1–6, 1974*. Schweizerbart'sche Verlagsbuchhandlung, Stuttgart, E. 310–316.

KAZMIN, V. 1972. *The Geology of Ethiopia*. Geological Survey of Ethiopia Report, Ministry of Mines, Addis Ababa, Ethiopia.

KENEA, N. H., EBINGER, C. J. & REX, D. C. 2001. Late Oligocene volcanism and extension in the southern Red Sea Hills, Sudan. *Journal of the Geological Society, London*, **158**, 285–294, http://doi.org/10.1144/jgs.158.2.285

KENNAN, P. S., MITCHELL, J. G. & MOHR, P. 1990. The Sagatu Ridge dyke swarm, Ethiopian rift margin: revised age and new Sr-isotopic data. *Journal of African Earth Sciences*, **11**, 39–42.

KIEFFER, B., ARNDT, N. *ET AL.* 2004. Flood and shield basalts from Ethiopia: magmas from the African Superswell. *Journal of Petrology*, **45**, 793–834.

LECHEMINANT, A. N. & HEAMAN, L. M. 1989. Mackenzie igneous events, Canada: middle Proterozoic hotspot magmatism associated with ocean opening. *Earth and Planetary Science Letters*, **96**, 38–48.

LENOIR, X., FÉRAUD, G. & GEOFFROY, L. 2003. High-rate flexure of the East Greenland volcanic margin: constraints from $^{40}Ar/^{39}Ar$ dating of basaltic dykes. *Earth and Planetary Science Letters*, **214**, 515–528.

LEROY, S., LUCAZEAU, F. *ET AL.* 2010. Contrasted styles of rifting in the eastern Gulf of Aden: a combined wide-angle, multichannel seismic, and heat flow survey. *Geochemistry, Geophysics, Geosystems*, **11**, Q07004, http://doi.org/10.1029/2009GC002963

LEROY, S., RAZIN, P. *ET AL*. 2012. From rifting to oceanic spreading in the Gulf of Aden: a synthesis. *Arabian Journal of Geosciences*, **5**, 859–901.

LIN, S.-C., KUO, B.-Y., CHIAO, L.-Y. & VAN KEKEN, P. E. 2005. Thermal plume models and melt generation in East Africa: a dynamic modeling approach. *Earth and Planetary Science Letters*, **237**, 175–192.

LISTER, J. R. & KERR, R. C. 1991. Fluid-mechanical models of crack propagation and their application to magma transport in dykes. *Journal of Geophysical Research*, **96**, 10 049–10 077.

MANIGHETTI, I., TAPPONNIER, P., COURTILLOT, V., GALLET, Y., JACQUES, E. & GILLOT, P.-Y. 2001. Strain transfer between disconnected, propagating rifts in Afar. *Journal of Geophysical Research*, **106**, 13 613–13 665.

MARTY, B., PIK, R. & YIRGU, G. 1996. Helium isotopic variations in Ethiopian plume lavas: nature of magmatic sources and limit on lower mantle contribution. *Earth and Planetary Science Letters*, **144**, 223–237.

MAXUS ETHIOPIA 1993. *Ogaden Concession Final Report*. Ethiopian Ministry of Mines & Energy unpublished report, Addis Ababa, Ethiopia.

MCDONOUGH, W. F. & SUN, S.-S. 1995. The composition of the Earth. *Chemical Geology*, **120**, 223–253.

MCQUARRIE, N., STOCK, J. M., VERDEL, C. & WERNICKE, B. P. 2003. Cenozoic evolution of Neotethys and implications for the causes of plate motions. *Geophysical Research Letters*, **30**, 2036, http://doi.org/10.1029/2003GL017992

MÈGE, D. & KORME, T. 2004*a*. Dyke swarm emplacement in the Ethiopian flood basalt province: not only a matter of stress. *Journal of Volcanology and Geothermal Research*, **132**, 283–310.

MÈGE, D. & KORME, T. 2004*b*. Fissure eruption of flood basalts from statistical analysis of dyke fracture length. *Journal of Volcanology and Geothermal Research*, **131**, 77–92.

MÈGE, D. & PURCELL, P. G. 2010. *Ethiopian Flood Basalt Province: 2. The Ogaden dyke swarm*. 6th International Dyke Conference Abstracts, Varanasi, India, 85.

MÈGE, D., GAUDIN, A. & MORIZET, Y. 2008. *Geology of Ogaden blocks 18-19-21, Ethiopia (Pexco concession): observations and preliminary results*. Pexco Exploration (East Africa) N. V. Report.

MÈGE, D., ARNAUD, N., DIOT, H., KORME, T. & SCHULTZ, R. A. 2010*a*. *Ethiopian Flood Basalt Province: 1. Dyke Swarms of Northwestern Ethiopia*. 6th International Dyke Conference Abstracts, Varanasi, India, 84.

MÈGE, D., PURCELL, P. & JOURDAN, J. 2010*b*. *Re-evaluation of Cenozoic Magmatism in the Northern Somali plate*. Abstract presented at the 23rd Réunion annuelle des sciences de la Terre, Bordeaux, France.

MÈGE, D., PURCELL, P., POCHAT, S. & GUIDAT, S. 2015. The landscape and landforms of the Ogaden, Southeast Ethiopia. *In*: BILLI, P. (ed.) *Landscapes and Landforms of Ethiopia*. World Geomorphological Landscape Series. Springer, Dordrecht, 323–348, http://doi.org/10.1007/978-94-017-8026-1_19

MOGHAZI, A-K. M. 2003. Geochemistry of a Tertiary continental basalt suite, Read Sea costal plain, Egypt: petrogenesis and characteristics of the mantle source region. *Geological. Magazine*, **140**, 11–24, http://doi.org/10.1017/S0016756802006994

MOHR, P. A. 1971. *Ethiopian Tertiary dike swarms*. Smithsonian Astrophysical Observatory Special Report, 339.

MOHR, P. A. 1975. Structural setting and evolution of Afar. *In*: PILGER, A. & ROSLER, A. (eds) *Proceedings of an International Symposium on the Afar Region and Related Rift Problems, held in Bad Bergzabern, F. R. Germany, April 1–6, 1974*. Schweizerbart'sche Verlagsbuchhandlung, Stuttgart, E, 27–37.

MOHR, P. A. 1978. Afar. *Annual Reviews of Earth and Planetary Sciences*, **6**, 145–172.

MOHR, P. 1983. Ethiopian flood basalt province. *Nature*, **303**, 577–584.

MOHR, P. 1991. Structure of Yemen Miocene dyke swarms and emplacement of coeval granite plutons. *Tectonophysics*, **198**, 203–221.

MOHR, P. A. & POTTER, E. C. 1976. The Sagatu Ridge dyke swarm, Ethiopian rift margin. *Journal of Volcanology and Geothermal Research*, **1**, 55–71.

MOHR, P. & ZANETTIN, B. 1988. The Ethiopian flood basalt province. *In*: MCDOUGALL, J. D. (ed.) *Continental Flood Basalts*. Kluwer Academic, Massachussetts, 63–110.

MORLEY, C. K., WESCOTT, W. A., STONE, D. M., HARPER, R. M., WIGGER, S. T. & KARANJA, F. M. 1992. Tectonic evolution of the northern Kenya rift. *Journal of the Geological Society, London*, **149**, 333–348, http://doi.org/10.1144/gsjgs.149.3.0333

MOSELEY, F. 1969. The Aden Traps of Dahla, Musaymir and Radfan, South Yemen. *Bulletin Volcanologique*, **33**, 889–909.

MOUFTI, M. R., MOGHAZI, A. M. & ALI, K. A. 2012. Geochemistry and Sr–Nd–Pb isotopic of the Harrat Al-Madinah volcanic field, Saudi Arabia. *Gondwana Research*, **21**, 670–689.

NELSON, W. R., FURMAN, T., VAN KEKEN, P. E., SHIREY, S. B. & HANAN, B. 2012. Os–Hf isotopic insight into mantle plume dynamics beneath the East African Rift System. *Chemical Geology*, **320–321**, 66–79.

ORIHASHI, Y., AL-JAILANI, A. & NAGAO, K. 1998. Dispersion of the Afar plume: implications from the spatiotemporal distribution of the Late Miocene to Recent volcanics, Southwestern Arabian Peninsula. *Gondwana Research*, **1**, 221–234.

PETCOVIC, H. L. & GRUNDER, A. L. 2003. Textural and thermal history of partial melting in tonalitic wallrock at the margin of a basalt dike, Wallowa Mountains, Oregon. *Journal of Petrology*, **44**, 2287–2312.

PIK, R., DENIEL, C., COULON, C., YIRGU, G., HOFMANN, C. & AYALEW, D. 1998. The northwestern Ethiopian plateau flood basalts: classification and spatial distribution of magma types. *Journal of Volcanology and Geothermal Research*, **81**, 91–111.

PIK, R., DENIEL, C., COULON, C., YIRGU, G. & MARTY, B. 1999. Isotopic and trace element signatures of Ethiopian flood basalts: evidence for plume–lithosphere interactions. *Geochimica et Cosmochimica Acta*, **63**, 2263–2279.

PIK, R., MARTY, B., CARIGNAN, J. & LAVÉ, J. 2003. Stability of the Upper Nile drainage network (Ethiopia) deduced from (U–Th)/He thermochronometry: implications for uplift and erosion of the Afar plume dome. *Earth and Planetary Science Letters*, **215**, 73–88, http://doi.org/10.1016/S0012-821X(03)00457-6

PIK, R., MARTY, B. & HILTON, D. R. 2006. How many mantle plumes in Africa? The geochemical point of view. *Chemical Geology*, **226**, 100–114.

PIK, R., MARTY, B., CARIGNAN, J., YIRGU, G. & AYALEW, T. 2008. Timing of East African Rift development in southern Ethiopia: implication for mantle plume activity and evolution of topography. *Geology*, **36**, 167–170, http://doi.org/10.1130/G24233A.1

PURCELL, P. G. 1975. Gravity anomalies over the Marda Fault Zone, Ethiopia. *Bulletin of the Geophysical Observatory (Ethiopia)*, **15**, 133–140.

PURCELL, P. G. 1976. The Marda Fault Zone, Ethiopia. *Nature*, **261**, 569–571.

PURCELL, P. G. 1981*a*. Phanerozoic sedimentary history and petroleum potential. *In*: CHEWAKA, S. & DE WITT, M. J. (eds) *Plate Tectonics and Metallogenesis: Some Guidelines to Ethiopian Mineral Deposits*. Ethiopian Institute of Geological Surveys Bulletin, **2**, 97–114.

PURCELL, P. G. 1981*b*. *The Bouguer Gravity Field of Ethiopia and the Tectonics of the East African Rift*. MSc thesis, University of Sydney, Australia.

RAPOLLA, A., CELLA, A. & DORRE, A. S. 1995. Gravity study of the crustal structures of Somalia along International Lithosphere Program intersects. *Journal of African Earth Science*, **20**, 263–74.

REIDEL, S. P. & TOLAN, T. L. 1992. Eruption and emplacement of flood basalt: an example from the large-volume Teepee Butte Member, Columbia River Basalt Group. *Geological Society of America Bulletin*, **104**, 1650–1671.

RENNE, P. R., MUNDIL, R., BALCO, G., MIN, K. & LUDWIG, K. 2010. Joint determination of ^{40}K decay constants and $^{40}Ar^*/^{40}K$ for the Fish Canyon sanidine standard, and improved accuracy for $^{40}Ar/^{39}Ar$ geochronology. *Geochimica et Cosmochimica Acta*, **74**, 5349–5367.

ROCHETTE, P., TAMRAT, E. *ET AL.* 1998. Magnetostratigraphy and timing of the Oligocene Ethiopian traps. *Earth and Planetary Science Letters*, **164**, 497–510.

ROGERS, N., MACDONALD, R., FITTON, J. G., GEORGE, R., SMITH, M. & BARREIRO, B. 2000. Two mantle plumes beneath the East African rift system: Sr, Nd and Pb isotope evidence from the Kenya Rift basalts. *Earth and Planetary Science Letters*, **176**, 387–400.

ROONEY, T. O., HANAN, B. B., GRAHAM, D. W., FURMAN, T., BLICHERT-TOFT, J. & SCHILLING, J.-G. 2012. Upper mantle pollution during Afar plume–continental rift interaction. *Journal of Petrology*, **53**, 365–389.

ROONEY, T. O., MOHR, P., DOSSO, L. & HALL, C. 2013. Geochemical evidence of mantle reservoir evolution during progressive rifting along the western Afar margin. *Geochimica et Cosmochimica Acta*, **102**, 65–88.

RUEGG, J.-C., LÉPINE, J. C., TARANTOLA, A. & LÉVÊQUE, J.-J. 1981. The Somalian earthquakes of May, 1980, East Africa. *Geophysical Research Letters*, **8**, 317–320.

SCHULTZ, R. A., MÈGE, D. & DIOT, H. 2008. Emplacement conditions of igneous dikes in Ethiopian Traps. *Journal of Volcanology and Geothermal Research*, **178**, 683–692, http://doi.org/10.1016/j.jvolgeores.2008.08.012

SEBAI, A., ZUMBO, V., FÉRAUD, G., BERTRAND, H., HUSSAIN, A. G., GIANNERINI, G. & CAMPREDON, R. 1991. $^{40}Ar/^{39}Ar$ dating of alkaline and tholeiitic magmatism of Saudi Arabia related to the early Red Sea rifting. *Earth and Planetary Science Letters*, **104**, 473–487.

SHACHNAI, E. 1972. *The Geology of Sheets NC37-12, NC38-9, Harar Province, Ethiopia*. Ministry of Mines Hydrogeology Department, Progress Report, Addis Ababa, Ethiopia.

SHACKLETON, R. M. 1996. The final collision zone between East and West Gondwana: where is it? *Journal of African Earth Sciences*, **23**, 271–287.

SHELL INTERNATIONALE PETROLEUM MIJ B. V. 1988. *Juba Concession Report*. Unpublished Report for Somalia Ministry of Mineral and Water Resources.

SINCLAIR PETROLEUM 1950. *Final Report of Exploration Drilling Program*. Unpublished report, Ogaden, Ethiopia

SOMMAVILLA, E., CARIF, S., SALAD, H. & FARAH, I. M. 1993. Neotectonic and geomorphological events in Central Somalia. *In*: ABBATE, E., SAGRI, M. & SASSI, F. P. (eds) *Geology and Mineral Resources of Somalia and Surrounding Regions*. Istituto Agronomico per l'Oltremare, Relazioni E Monografie Agrarie Subtropicali e Tropicale, Florence, Italy, **113A**, 389–396.

STRAUB, A. 1958. *A Report of Investigations for Oil in Ethiopia*. Unpublished report, Ethiopia Ministry of Mines Files, Addis Ababa, Ethiopia.

TEFERA, M., CHERNET, T. & HARO, W. 1996. *Geological map of Ethiopia, 1:2,000,000 scale*, 2nd edn. Geological Survey of Ethiopia, Addis Ababa, Ethiopia.

THORDARSON, T. & SELF, S. 1998. The Roza Member, Columbia River Basalt Group: a gigantic pahoehoe lava flow field formed by endogenous processes? *Journal of Geophysical Research*, **103**, 27 411–27 445.

UKSTINS, I. A., RENNE, P. R., WOLFENDEN, E., BAKER, J., AYALEW, D. & MENZIES, M. 2002. Matching conjugate volcanic rifted margins: $^{40}Ar/^{39}Ar$ chronostratigraphy of pre- and syn-rift bimodal flood volcanism in Ethiopia and Yemen. *Earth and Planetary Science Letters*, **198**, 289–306.

UKSTINS PEATE, I., BAKER, J. A. *ET AL.* 2005. Volcanic stratigraphy of large-volume silicic pyroclastic eruptions during Oligocene Afro-Arabian volcanism in Yemen. *Bulletin of Volcanology*, **68**, 135–156.

UTS GEOPHYSICS 2008. Logistics Report for a Detailed Airborne Magnetic and Digital Terrain Survey for the Ogaden Basin Project on behalf of Pexco Exploration (East Africa) N.V. Unpublished report, Petroleum Department, Ethiopian Ministry of Mines.

VOLKER, F., ALTHERR, R., JOCHUM, K.-P. & MCCULLOCH, M. T. 1997. Quaternary volcanic activity of the southern Red Sea: new data and assessment of models on magma sources and Afar plume–lithosphere interaction. *Tectonophysics*, **278**, 15–29.

VYE-BROWN, C., SELF, S. & BARRY, T. L. 2013. Architecture and emplacement of flood basalt fields: case studies from the Columbia River Basalt Group, NW USA. *Bulletin of Volcanology*, **75**, 697, http://doi.org/10.1007/s00445-013-0697-2

WALL, M., CARTWRIGHT, J., DAVIES, R. & MCGRANDLE, A. 2009. 3D seismic imaging of a Tertiary dyke swarm in the Southern North Sea. *Basin Research*, **10**, 1–14.

WATCHORN, F., NICHOLS, G. J. & BOSENCE, D. W. J. 1998. Rift-related sedimentation and stratigraphy, southern Yemen (Gulf of Aden). *In*: PURSER, B. H. & BOSENCE, D. W. J. (eds) *Sedimentation and Tectonics of Rift Basins: Red Sea–Gulf of Aden*. Chapman and Hall, London, 165–189.

WHITE, R. & MCKENZIE, D. 1989. Magmatism at rift zones: the generation of volcanic continental margins and flood basalts. *Journal of Geophysical Research*, **94**, 7685–7729.

WOLELA, A. 2004. Sedimentology, depositional environments and basin evolution of coal and oil shale-bearing sediments in the Delbi-Moye Basin, Southwestern Ethiopia. *Ethiopian Journal of Science*, **27**, 45–60.

WOLFENDEN, E., EBINGER, C., YIRGU, G., DEINO, A. & AYALEW, D. 2004. Evolution of the northern Main Ethiopian rift: birth of a triple junction. *Earth and Planetary Science Letters*, **224**, 213–228.

WOLFENDEN, E., EBINGER, C., YIRGU, G., RENNE, P. R. & KELLEY, S. P. 2005. Evolution of a volcanic rifted margin: Southern Red Sea, Ethiopia. *Geological Society of America Bulletin*, **117**, 846–864.

WOOD, C. A. 1979. The Marda Fault Zone and the opening of the Red Sea. *In*: EL-BAZ, F. & WARNER, D. M. (eds) *Apollo/Soyuz Test Project, Summary Science Project, Volume 2: Earth Observations and Photography*. NASA SP-412, 29–36.

WRIGHT, T. J., EBINGER, C., BIGGS, J., AYELE, A., YIRGU, G., KEIR, D. & STORK, A. 2006. Magma-maintained rift segmentation at continental rupture in the 2005 Afar dyking episode. *Nature*, **442**, 291–294, http://doi.org/10.1038/nature04978

ZANETTIN, B. & JUSTIN-VISENTIN, E. 1975. Tectonical and volcanological evolution of the western Afar margin, Ethiopia. *In*: PILGER, A. & ROSLER, A. (eds) *Proceedings of an International Symposium on the Afar Region and Related Rift Problems, held in Bad Bergzabern, F. R. Germany, April 1–6, 1974*. Schweizerbart'sche Verlagsbuchhandlung, Stuttgart, E.

ZIV, A., RUBIN, A. M. & AGNON, A. 2000. Stability of dike intrusion along the preexisting fractures. *Journal of Geophysical Research*, **105**, 5947–5961.

ZOBACK, M. L., MCKEE, E. H., BLAKELY, R. J. & THOMPSON, G. A. 1994. The northern Nevada rift: regional tectono-magmatic relations and middle Miocene stress direction. *Geological Society of America Bulletin*, **106**, 371–382.

ZUMBO, W., FÉRAUD, G., BERTRAND, H. & CHAZOT, G. 1995. $^{40}Ar/^{39}Ar$ chronology of Tertiary magmatic activity in Southern Yemen during the early Red Sea–Aden rifting. *Journal of Volcanology and Geothermal Research*, **65**, 265–279.

Supplementary material 1 (see File 2). Geological map of the Marda Fault Zone and surroundings. The map has been prepared from satellite imagery (Landsat ETM+, and sub-metre resolution satellite images) and reinterpretation of earlier maps (Tasfai 1975; BEICIP; 1985; Tefera *et al.* 1996; Earth Satellite Corporation 2004; Yihune and Haro 2010). The reported fold hinge lines and dip angles have been redrawn from Tasfai (1975), who used stereoscopic analysis of aerial photographs for geological interpretation. The NW-SE fracture lines are parallel to the Precambrian fabric. The latter is frequently subparallel to the maximum topographic slope, resulting in unclear tectonic control of Ogaden rivers flowing to the SE. The topographic contours (separation 200 m) have been extracted from METI/NASA/ASTER Global DEM.

Supplementary material 2a. Argon dating analytical protocol.

The plagioclase crystals were separated using a Frantz magnetic separator, and then carefully hand-picked under a binocular microscope. The selected groundmass and plagioclase were further leached in diluted HF for one minute and then thoroughly rinsed with distilled water in an ultrasonic cleaner.

The samples were irradiated in 2009 (irradiation I10t2h) and again in 2011 (irradiation I12t2h). The samples were loaded into individual large wells of 1.9 cm diameter and 0.3 cm depth aluminum discs. These wells were bracketed by small wells that included Fish Canyon sanidine (FCs) used as a neutron fluence monitor for which an age of 28.305 ± 0.036 Ma (1σ) was adopted (Renne *et al.* 2010). For both irradiations, the discs were Cd-shielded (to minimize undesirable nuclear interference reactions) and irradiated for 2 hours in the Hamilton McMaster University nuclear reactor (Canada) in position 5C. The mean J-values were computed from standard grains within the small pits and determined as the average and standard deviation of J-values of the small wells for each irradiation disc. Mass discrimination was monitored using an automated air pipette and calibrated relative to an air ratio of 298.56 ± 0.31 (Lee *et al.* 2006). The J-value and mass discrimination value are given for each sample in the raw analytical data (Appendix 2b). The correction factors for interfering isotopes were $(^{39}Ar/^{37}Ar)_{Ca} = 7.30x10^{-4}$ (± 11%), $(^{36}Ar/^{37}Ar)_{Ca} = 2.82x10^{-4}$ (± 1%) and $(^{40}Ar/^{39}Ar)_{K} = 6.76x10^{-4}$ (± 32%).

The $^{40}Ar/^{39}Ar$ analyses were performed at the Western Australian Argon Isotope Facility at Curtin University. The sample was step-heated in a double vacuum high-frequency Pond

Engineering© furnace. The gas was purified in a stainless steel extraction line using two AP10 and one GP50 SAES getters and a liquid nitrogen condensation trap. Ar isotopes were measured in static mode using a MAP 215-50 mass spectrometer (resolution of ~400; sensitivity of $4x10^{-14}$ mol/V) with a Balzers SEV 217 electron multiplier mostly using 9 to 10 cycles of peak-hopping.

Data acquisition used an Argus program written by M. O. McWilliams and ran under a LabView environment. The raw data were processed using the ArArCALC software (Koppers 2002) and the ages have been calculated using the decay constants recommended by Renne *et al.* (2010). Furnace blanks were monitored every 3 samples and typical ^{40}Ar blanks range from 1 x 10^{-16} to 2 x 10^{-16} mol. Ar isotopic data corrected for blank, mass discrimination and radioactive decay are given in Appendix 2b. Individual errors in Appendix 2b are given at the 1σ level. Our criteria for the determination of a plateau require that they must include at least 70% of ^{39}Ar, and are distributed over a minimum of 3 consecutive steps agreeing at 95% confidence level and satisfying a probability of fit (P) of at least 0.05. Plateau ages (Table 2 and Fig. 7) are given at the 2σ level and are calculated using the mean of all the plateau steps, each weighted by the inverse variance of their individual analytical error. Mini-plateaus are defined similarly except that they include between 50% and 70% of ^{39}Ar and are given much less significance compared to a plateau. Inverse isochrons include the maximum number of steps with a probability of fit ≥ 0.05. All sources of uncertainties are included in the calculation.

Supplementary material 2b (see File 3). Ar isotopic data corrected from baseline, background, mass discrimination interference corrections and radioactive decay. Values in red indicate negative values. Negative values are expected when measured values are around background level. Step ages calculated after Renne *et al.* (2010).

Supplementary material 3a (see File 4). Petrographic description of representative samples of the Ogaden Dyke Swarm.

Supplementary material 3b. Analytical protocol used for geochemistry.

Each sample was carefully prepared to extract only the freshest parts of the rocks prior powdering. Major and trace elements were analysed respectively by ICP-OES (Thermo I-CAP) and ICP-MS (Bruker 820MS) at the Laboratoire de Planétologie et Géodynamique in Nantes University (France). Major elements were analysed on 125 mg aliquot of samples following the procedure described by Cotten *et al.* (1995), and trace element were analysed following the Bézos *et al.* (2009) method. The results are reported in Table 3. Appendix 4 provides results for geo-referenced materials BCR-2 recalculated with calibration curves obtained with standards AGV62, BE-N, BHVO-2, W-2, JB-2, BIR-1, and BCR-2 for both major and trace elements. Also reported in this table are results for sample MQR8 that was analyzed during each analytical session in order to monitor data processing reproducibility.

Supplementary material 4 (see File 5). Major and trace analyses of georeferenced materials BCR-2 for the Ogaden Dyke Swarm samples.

References

BEICIP 1985. Geological map of the Ogaden and surrounding area. Addis Ababa, Ethiopia, 1:1,000,000. Ministry of Mines and Energy, Addis Ababa, Ethiopia.

BÉZOS, A., ESCRIG, S., LANGMUIR, C. H., MICHAEL, P. J. & ASIMOW, P. D. 2009. Origins of chemical diversity of back-arc basin basalts: A segment-scale study Eastern Lau Spreading Center. *Journal of Geophysical Research*, **114**, B06212, doi:10.1029/2008JB005924.

COTTEN, J., LE DEZ, A., BAU, M. *ET AL.* 1995. Origin of anomalous rare-earth element and yttrium enrichments in subaerially exposed basalts: Evidence from French Polynesia. *Chemical Geology*, **119**, 115–138.

EARTH SATELLITE CORPORATION, 2004. Photogeologic and hydrocarbon microseepage mapping, Ogaden Basin, Ethiopia. Petronas Caligari SDN BHD, Mapsheet 2.

KOPPERS, A. A. P. 2002. ArArCALC-software for $^{40}Ar/^{39}Ar$ age calculations. *Computers & Geosciences*, **28**, 605–619.

LEE, J.-Y., MARTI, K., SEVERINGHAUS, J. P., KAWAMURA, K., YOO, H.-S., LEE, J. B. & KIM, J. S. 2006. A redetermination of the isotopic abundance of atmospheric Ar. *Geochimica et Cosmochimica Acta*, **70**, 4507–4512.

RENNE, P. R. MUNDIL, R. BALCO, G., MIN, K. & LUDWIG, K. R. 2010. Joint determination of ^{40}K decay constants and $^{40}Ar^*/^{40}K$ for the Fish Canyon sanidine standard, and improved accuracy for $^{40}Ar/^{39}Ar$ geochronology. *Geochimica et Cosmochimica Acta*, **74**, 5349–5367.

TASFAI, 1975. Photogeologic interpretation, OC-3 & EL-8, scale 1:420,000. Whitestone Ethiopia Petroleum Co., 1 map.

TEFERA, M., CHERNET, T. & HARO, W. 1996. *Geological map of Ethiopia, 1:2,000,000*, second edition. Addis Ababa, Ethiopia, Geological Survey of Ethiopia.

YIHUNE, T. & HARO, W. 2010. Geological map of Harar area, NC 38-9. Ethiopian Mapping Agency, 1:250,000 Regional Geologic Map Series.

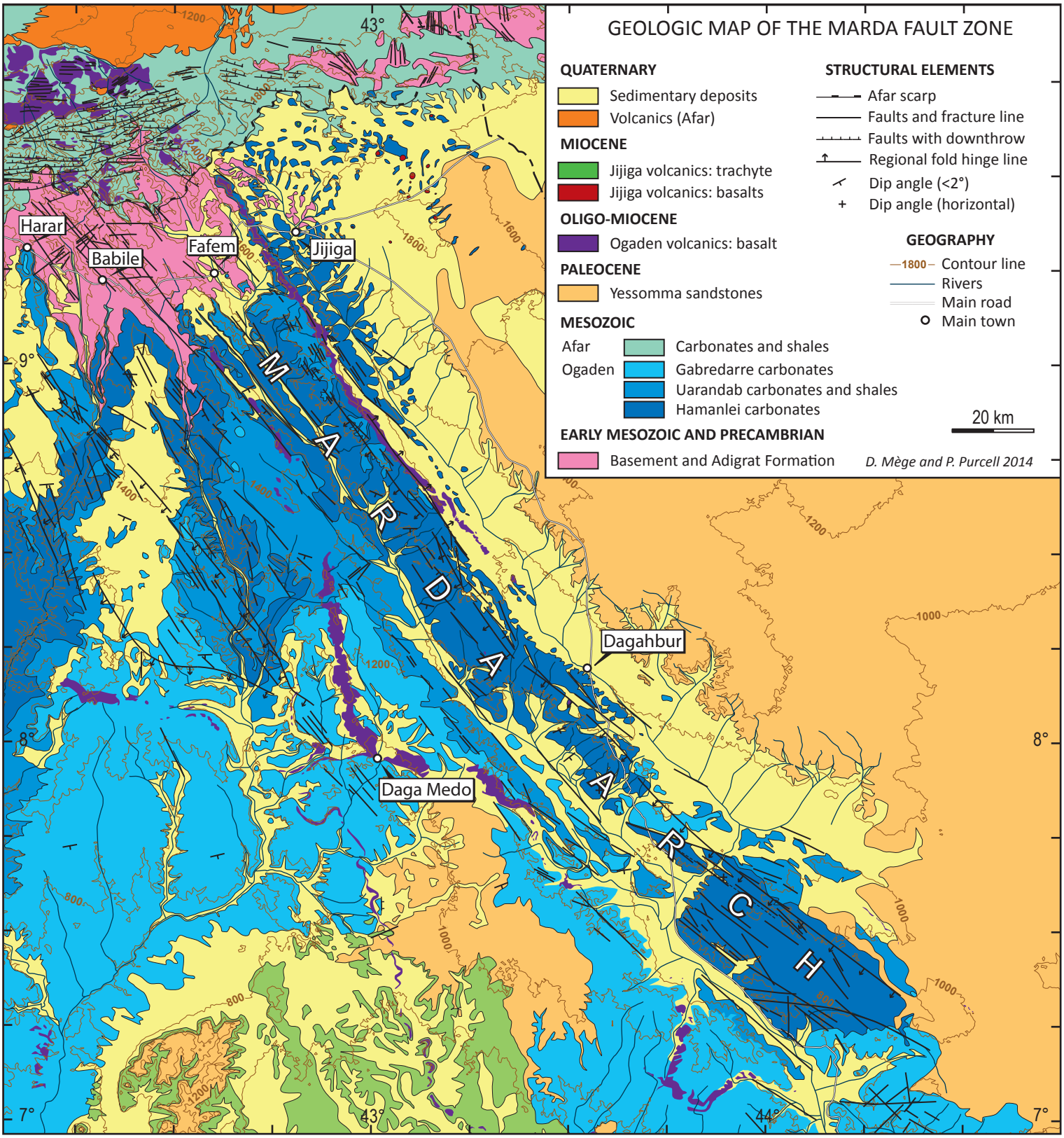
GEOLOGIC MAP OF THE MARDA FAULT ZONE
QUATERNARY
Sedimentary deposits
Volcanics (Afar)
MIOCENE
Jijiga volcanics: trachyte
Jijiga volcanics: basalts
OLIGO-MIOCENE
Ogaden volcanics: basalt
PALEOCENE
Yessomma sandstones
MESOZOIC
Afar
Ogaden
Carbonates and shales
Gabredarre carbonates
Uarandab carbonates and shales
Hamanlei carbonates
EARLY MESOZOIC AND PRECAMBRIAN
Basement and Adigrat Formation
STRUCTURAL ELEMENTS
Afar scarp
Faults and fracture line
Faults with downthrow
Regional fold hinge line
Dip angle (<2°)
Dip angle (horizontal)
GEOGRAPHY
1800 Contour line
Rivers
Main road
Main town
20 km
D. Mège and P. Purcell 2014
Harar
Babile
Fafem
Jijiga
Dagahbur
Daga Medo
MARDA FAULT
AARCH
43°
44°
9°
8°
7°

,,,,,,,,,,,,
Incremental
,,,,,,,,(Ma),,(%),(%),,
11,,,,,,,,,,,,
0B11946D,600.00 W,4, 0.000125, 0.087497, 0.000094, 0.007806, 0.143702,24.47,± 1.66, 79.49, 10.24,0.038,± 0.003
0B11947D,650.00 W,4, 0.000227, 0.146221, 0.000152, 0.012191, 0.224368,24.47,± 1.08, 77.01, 15.99,0.036,± 0.002
0B11948D,700.00 W,4, 0.000295, 0.131524, 0.000206, 0.010543, 0.191029,24.09,± 1.72, 68.63, 13.83,0.034,± 0.002
0B11949D,775.00 W,4, 0.000606, 0.144683, 0.000600, 0.009524, 0.171799,23.98,± 2.19, 48.97, 12.49,0.028,± 0.002
0B11950D,850.00 W,4, 0.000254, 0.104008, 0.001306, 0.006429, 0.120839,24.98,± 2.29, 61.70, 8.43,0.027,± 0.002
0B11951D,925.00 W,, 0.000176, 0.105577, 0.002889, 0.005846, 0.095683,21.77,± 2.26, 64.78, 7.67,0.024,± 0.002
0B11952D,1000.00 W,, 0.000195, 0.112835, 0.002722, 0.005548, 0.075547,18.13,± 2.27, 56.69, 7.28,0.021,± 0.001
0B11953D,1075.00 W,, 0.000699, 0.576394, 0.003928, 0.005788, 0.077985,17.94,± 2.74, 27.42, 7.59,0.004,± 0.000
0B11954D,1150.00 W,, 0.000627, 2.108094, 0.001952, 0.008925, 0.140328,20.92,± 3.36, 43.09, 11.71,0.002,± 0.000
0B11955D,1225.00 W,, 0.000423, 0.453414, 0.000381, 0.003484, 0.070156,26.75,± 9.11, 35.94, 4.57,0.003,± 0.000
0B11956D,1300.00 W,, 0.000971, 0.011515, 0.000015, 0.000145, 0.000000,0.00,± 0.00, 0.00, 0.19,0.005,± 0.002
,,,,,,,,,,,,
G17,,,,,,,,,,,,
0B11813D,600.00 W,, 0.000214, 0.110967, 0.000016, 0.008591, 0.163686,24.33,± 2.67, 72.11, 10.66,0.033,± 0.002
0B11814D,650.00 W,, 0.000267, 0.105022, 0.000013, 0.006829, 0.131422,24.57,± 3.38, 62.49, 8.48,0.028,± 0.002
0B11815D,700.00 W,, 0.000587, 0.076307, 0.000015, 0.004267, 0.084300,25.22,± 5.22, 32.69, 5.30,0.024,± 0.002
0B11816D,775.00 W,, 0.000383, 0.075365, 0.000030, 0.003663, 0.069885,24.36,± 5.84, 38.16, 4.55,0.021,± 0.001
0B11817D,850.00 W,4, 0.000390, 0.054502, 0.000064, 0.003140, 0.045178,18.40,± 6.99, 28.14, 3.90,0.025,± 0.002
0B11818D,925.00 W,4, 0.000084, 0.052753, 0.000100, 0.003267, 0.037905,14.85,± 6.17, 60.57, 4.06,0.027,± 0.002
0B11819D,1000.00 W,4, 0.000116, 0.065053, 0.000160, 0.003760, 0.037926,12.92,± 5.66, 52.61, 4.67,0.025,± 0.002
0B11820D,1075.00 W,4, 0.000766, 0.874845, 0.000632, 0.023223, 0.291060,16.04,± 1.19, 56.25, 28.83,0.011,± 0.001
0B11821D,1150.00 W,4, 0.000241, 1.421054, 0.000410, 0.023129, 0.324005,17.92,± 1.08, 81.95, 28.71,0.007,± 0.000
0B11822D,1225.00 W,4, 0.000465, 0.034551, 0.000000, 0.000628, 0.008982,18.30,± 32.38, 6.13, 0.78,0.008,± 0.001
0B11823D,1300.00 W,, 0.001581, 0.001181, 0.000009, 0.000062, 0.000000,0.00,± 0.00, 0.00, 0.08,0.023,± 0.024
,,,,,,,,,,,,
W3.4,,,,,,,,,,,,
0B9774D, 600 °C,, 0.002227, 0.041800, 0.000027, 0.008962, 0.039905,6.01,± 4.56, 5.72, 5.35,0.092,± 0.006
0B9775D, 650 °C,, 0.003481, 0.083774, 0.000037, 0.014472, 0.082018,7.64,± 3.52, 7.39, 8.64,0.074,± 0.004
0B9776D, 700 °C,, 0.003738, 0.103479, 0.000000, 0.014366, 0.141805,13.29,± 3.64, 11.38, 8.58,0.060,± 0.003

0B9777D, 775 °C,, 0.005066, 0.141962, 0.000032, 0.015631, 0.223650,19.23,± 4.04, 13.00, 9.33,0.047,± 0.003
0B9778D, 850 °C,, 0.007206, 0.169483, 0.000099, 0.017660, 0.250653,19.08,± 5.17, 10.53, 10.54,0.045,± 0.002
0B9779D, 925 °C,, 0.008801, 0.151596, 0.000038, 0.019100, 0.297496,20.92,± 5.50, 10.27, 11.40,0.054,± 0.003
0B9780D,1000 °C,, 0.011302, 0.119409, 0.000200, 0.019528, 0.349042,23.99,± 6.66, 9.46, 11.66,0.070,± 0.004
0B9781D,1075 °C,, 0.014479, 0.193897, 0.000226, 0.018446, 0.348847,25.37,± 8.97, 7.54, 11.01,0.041,± 0.002
0B9782D,1150 °C,, 0.028262, 2.332053, 0.000479, 0.033556, 0.702781,28.08,± 9.43, 7.76, 20.03,0.006,± 0.000
0B9783D,1225 °C,, 0.003431, 0.475520, 0.000000, 0.005120, 0.091448,23.97,± 9.10, 8.27, 3.06,0.005,± 0.000
0B9784D,1300 °C,, 0.001086, 0.050215, 0.000032, 0.000657, 0.012689,25.89,± 33.92, 3.80, 0.39,0.006,± 0.001

,,,,,,,,,,,,

W1.1,,,,,,,,,,,,

0B9785D, 600 °C,4, 0.000137, 0.055913, 0.000023, 0.007397, 0.140436,25.37,± 1.69, 77.58, 6.20,0.057,± 0.003
0B9786D, 650 °C,4, 0.000316, 0.131080, 0.000008, 0.015482, 0.285317,24.63,± 1.03, 75.35, 12.97,0.051,± 0.003
0B9787D, 700 °C,4, 0.000316, 0.160998, 0.000013, 0.018840, 0.350048,24.83,± 0.71, 78.96, 15.79,0.050,± 0.003
0B9788D, 775 °C,4, 0.000457, 0.147190, 0.000037, 0.018381, 0.343412,24.97,± 0.92, 71.76, 15.40,0.054,± 0.003
0B9789D, 850 °C,4, 0.000501, 0.156713, 0.000014, 0.014123, 0.266501,25.22,± 1.25, 64.30, 11.84,0.039,± 0.002
0B9790D, 925 °C,4, 0.000464, 0.172326, 0.000066, 0.011235, 0.209416,24.91,± 1.54, 60.41, 9.42,0.028,± 0.002
0B9791D,1000 °C,4, 0.000509, 0.167389, 0.000115, 0.008747, 0.157621,24.09,± 1.79, 51.16, 7.33,0.022,± 0.001
0B9792D,1075 °C,4, 0.000660, 0.218464, 0.000232, 0.008344, 0.135299,21.69,± 6.78, 40.95, 6.99,0.016,± 0.001
0B9793D,1150 °C,4, 0.001557, 1.407967, 0.000457, 0.009950, 0.171056,22.99,± 6.12, 27.10, 8.34,0.003,± 0.000
0B9794D,1225 °C,4, 0.000487, 1.115212, 0.000052, 0.006299, 0.107926,22.91,± 9.19, 42.87, 5.28,0.002,± 0.000
0B9795D,1300 °C,4, 0.000273, 0.035001, 0.000003, 0.000528, 0.015917,40.10,± 87.97, 16.46, 0.44,0.006,± 0.002

,,,,,,,,,,,,

Ma03b,,,,,,,,,,,,

2B20385D, 550 °C,4, 0.000049, 0.021448, 0.000000, 0.002144, 0.038272,22.46,± 3.31, 72.31, 3.78,0.0430,± 0.0065
2B20386D, 600 °C,4, 0.000061, 0.037196, 0.000000, 0.003300, 0.065612,25.00,± 2.35, 78.37, 5.82,0.0381,± 0.0040
2B20387D, 650 °C,4, 0.000053, 0.039325, 0.000000, 0.003145, 0.064847,25.91,± 2.50, 80.35, 5.54,0.0344,± 0.0034
2B20388D, 700 °C,4, 0.000054, 0.042857, 0.000000, 0.003501, 0.070198,25.21,± 2.26, 81.32, 6.17,0.0351,± 0.0039
2B20389D, 775 °C,4, 0.000085, 0.059846, 0.000019, 0.005295, 0.102948,24.45,± 1.47, 80.20, 9.33,0.0380,± 0.0037
2B20390D, 850 °C,4, 0.000064, 0.055666, 0.000034, 0.004324, 0.083177,24.19,± 2.06, 81.40, 7.62,0.0334,± 0.0032
2B20391D, 925 °C,4, 0.000042, 0.046067, 0.000053, 0.002715, 0.047769,22.14,± 2.75, 79.24, 4.79,0.0253,± 0.0026
2B20392D,1000 °C,4, 0.000354, 0.201409, 0.000110, 0.015364, 0.284380,23.28,± 0.68, 72.91, 27.08,0.0328,± 0.0028
2B20393D,1020 °C,4, 0.000045, 0.077856, 0.000019, 0.001721, 0.030693,22.44,± 5.01, 69.52, 3.03,0.0095,± 0.0009
2B20394D,1040 °C,4, 0.000066, 0.208080, 0.000014, 0.003613, 0.065958,22.96,± 2.28, 77.06, 6.37,0.0075,± 0.0007

2B20395D,1060 °C,4, 0.000057, 0.283846, 0.000015, 0.003729, 0.066542,22.45,± 2.20, 79.66, 6.57,0.0056,± 0.0005
2B20396D,1080 °C,4, 0.000040, 0.215840, 0.000010, 0.002637, 0.049989,23.84,± 3.12, 80.61, 4.65,0.0053,± 0.0005
2B20397D,1100 °C,4, 0.000023, 0.083499, 0.000007, 0.001132, 0.020469,22.74,± 6.56, 74.51, 2.00,0.0058,± 0.0006
2B20398D,1250 °C,4, 0.000062, 0.256810, 0.000012, 0.003907, 0.078051,25.11,± 2.47, 80.71, 6.89,0.0065,± 0.0006
2B20399D,1400 °C,4, 0.000011, 0.018035, 0.000000, 0.000210, 0.003887,23.25,± 38.04,680.82, 0.37,0.0050,± 0.0008
,,,,,,,,,,,,
04a,,,,,,,,,,,,
0B11787D,600.00 W,4, 0.000413, 0.221127, 0.000734, 0.040293, 0.828283,27.05,± 0.65, 87.16, 16.90,0.078,± 0.005
0B11788D,650.00 W,4, 0.000335, 0.193638, 0.000525, 0.034965, 0.707999,26.64,± 0.61, 87.74, 14.67,0.078,± 0.005
0B11789D,700.00 W,4, 0.000415, 0.146029, 0.000499, 0.026159, 0.518733,26.10,± 0.90, 80.89, 10.97,0.077,± 0.005
0B11790D,775.00 W,4, 0.000447, 0.141061, 0.000979, 0.021300, 0.428447,26.47,± 1.11, 76.41, 8.93,0.065,± 0.004
0B11791D,850.00 W,4, 0.000485, 0.107829, 0.001488, 0.015049, 0.290717,25.43,± 1.81, 66.97, 6.31,0.060,± 0.004
0B11792D,925.00 W,4, 0.001077, 0.108588, 0.002284, 0.018184, 0.349660,25.31,± 1.55, 52.35, 7.63,0.072,± 0.005
0B11793D,1000.00 W,4, 0.001856, 0.102599, 0.002511, 0.019306, 0.385641,26.29,± 2.06, 41.28, 8.10,0.081,± 0.005
0B11794D,1075.00 W,4, 0.003182, 0.356168, 0.005200, 0.022999, 0.476689,27.27,± 2.27, 33.64, 9.65,0.028,± 0.002
0B11795D,1150.00 W,4, 0.006748, 2.863416, 0.005324, 0.034941, 0.700275,26.37,± 2.39, 25.99, 14.66,0.005,± 0.000
0B11796D,1225.00 W,4, 0.000864, 0.307790, 0.000410, 0.005076, 0.115677,29.96,± 6.36, 31.18, 2.13,0.007,± 0.000
0B11797D,1300.00 W,4, 0.002293, 0.007066, 0.000018, 0.000121, 0.004634,50.15,± 358.30, 0.68, 0.05,0.007,± 0.003
,,,,,,,,,,,,
41c,,,,,,,,,,,,
0B11900D, 600 °C,, 0.000366, 0.104514, 0.000960, 0.020073, 0.408168,26.61,± 0.72, 79.04, 11.38,0.083,± 0.006
0B11901D, 650 °C,, 0.000355, 0.132814, 0.000627, 0.017380, 0.351034,26.43,± 0.96, 76.99, 9.86,0.056,± 0.004
0B11902D, 700 °C,, 0.000352, 0.151311, 0.000588, 0.017507, 0.347523,25.98,± 0.90, 76.95, 9.93,0.050,± 0.003
0B11903D, 775 °C,, 0.001198, 0.226753, 0.001340, 0.024066, 0.447875,24.37,± 1.03, 55.86, 13.65,0.046,± 0.003
0B11904D, 850 °C,, 0.000430, 0.155185, 0.002379, 0.017652, 0.255362,18.97,± 0.71, 66.76, 10.01,0.049,± 0.003
0B11905D, 925 °C,, 0.000184, 0.095904, 0.002640, 0.011613, 0.119129,13.47,± 1.17, 68.61, 6.58,0.052,± 0.004
0B11906D,1000 °C,, 0.000163, 0.122288, 0.002669, 0.010229, 0.075465,9.70,± 1.34, 61.05, 5.80,0.036,± 0.002
0B11907D,1075 °C,, 0.000640, 0.910990, 0.003936, 0.014128, 0.188196,17.48,± 1.30, 49.86, 8.01,0.007,± 0.000
0B11908D,1150 °C,, 0.000964, 2.370779, 0.005862, 0.041153, 0.658099,20.96,± 0.74, 69.79, 23.33,0.007,± 0.000
0B11909D,1225 °C,, 0.000292, 0.112448, 0.000120, 0.002350, 0.041159,22.94,± 7.21, 32.33, 1.33,0.009,± 0.001
0B11910D,1300 °C,, 0.001789, 0.009913, 0.000000, 0.000208, 0.000000,0.00,± 0.00, 0.00, 0.12,0.009,± 0.002
,,,,,,,,,,,,
Incremental

,,,,,,,,(Ma),,(%),(%),,
MQR7a,,,,,,,,,,,,
2B21294D, 550 °C,4, 0.000056, 0.010883, 0.000000, 0.001233, 0.024398,24.80,± 6.46, 59.36, 1.65,0.0487,± 0.0306
2B21295D, 600 °C,4, 0.000227, 0.021712, 0.000000, 0.002685, 0.060034,27.98,± 3.78, 46.97, 3.59,0.0532,± 0.0177
2B21296D, 650 °C,4, 0.000706, 0.031590, 0.000000, 0.003518, 0.077074,27.42,± 4.32, 26.76, 4.71,0.0479,± 0.0152
2B21297D, 700 °C,4, 0.000528, 0.036623, 0.000005, 0.003867, 0.075187,24.36,± 3.00, 32.28, 5.17,0.0454,± 0.0101
2B21298D, 775 °C,4, 0.000439, 0.044203, 0.000009, 0.005283, 0.106837,25.33,± 2.66, 44.89, 7.07,0.0514,± 0.0091
2B21299D, 850 °C,4, 0.000215, 0.047008, 0.000021, 0.004737, 0.089586,23.70,± 2.24, 58.26, 6.34,0.0433,± 0.0084
2B21300D, 925 °C,4, 0.000175, 0.036020, 0.000020, 0.003054, 0.048319,19.85,± 9.47, 48.07, 4.09,0.0365,± 0.0068
2B21301D,1000 °C,4, 0.000947, 0.274836, 0.000112, 0.023518, 0.469500,25.01,± 0.92, 62.42, 31.46,0.0368,± 0.0043
2B21302D,1020 °C,4, 0.000223, 0.180984, 0.000024, 0.006581, 0.131403,25.01,± 2.17, 66.34, 8.81,0.0156,± 0.0019
2B21303D,1040 °C,4, 0.000225, 0.447641, 0.000034, 0.009333, 0.187797,25.21,± 1.33, 73.65, 12.49,0.0090,± 0.0010
2B21304D,1060 °C,4, 0.000094, 0.285094, 0.000021, 0.004481, 0.089386,24.99,± 2.39, 76.18, 6.00,0.0068,± 0.0008
2B21305D,1080 °C,4, 0.000055, 0.114828, 0.000017, 0.001952, 0.036013,23.12,± 4.66, 68.70, 2.61,0.0073,± 0.0009
2B21306D,1100 °C,4, 0.000022, 0.057213, 0.000000, 0.001007, 0.021614,26.87,± 9.47, 76.70, 1.35,0.0076,± 0.0012
2B21307D,1250 °C,4, 0.000137, 0.172443, 0.000008, 0.003149, 0.064755,25.75,± 3.33, 61.23, 4.21,0.0079,± 0.0010
2B21308D,1400 °C,4, 0.000070, 0.023714, 0.000002, 0.000345, 0.007075,25.68,± 31.62, 51.47, 0.46,0.0063,± 0.0015
,,,,,,,,,,,,
MQR8b,,,,,,,,,,,,
2B21406D, 580 °C,, 0.000011, 0.017776, 0.000000, 0.001702, 0.041444,30.38,± 3.28, 92.48, 4.45,0.0412,± 0.0155
2B21407D, 650 °C,, 0.000073, 0.040632, 0.000010, 0.004404, 0.096237,27.29,± 1.55, 81.56, 11.51,0.0466,± 0.0103
2B21408D, 720 °C,, 0.000129, 0.052948, 0.000003, 0.004529, 0.096334,26.57,± 1.57, 71.38, 11.83,0.0368,± 0.0063
2B21409D, 800 °C,, 0.000127, 0.048637, 0.000012, 0.003700, 0.076166,25.72,± 2.12, 66.80, 9.67,0.0327,± 0.0072
2B21410D, 850 °C,4, 0.000011, 0.010088, 0.000014, 0.000682, 0.011494,21.07,± 8.49, 78.07, 1.78,0.0291,± 0.0173
2B21411D, 925 °C,4, 0.000012, 0.010721, 0.000012, 0.000543, 0.010525,24.23,± 10.91, 73.91, 1.42,0.0218,± 0.0120
2B21412D,1000 °C,4, 0.000205, 0.076212, 0.000047, 0.003204, 0.054455,21.26,± 2.69, 47.04, 8.37,0.0181,± 0.0027
2B21413D,1020 °C,4, 0.000143, 0.171502, 0.000053, 0.005434, 0.100694,23.17,± 1.56, 70.25, 14.20,0.0136,± 0.0017
2B21414D,1040 °C,4, 0.000219, 0.491404, 0.000093, 0.009082, 0.162846,22.42,± 1.30, 71.37, 23.73,0.0079,± 0.0009
2B21415D,1060 °C,4, 0.000087, 0.260888, 0.000021, 0.003339, 0.059414,22.25,± 2.69, 69.54, 8.73,0.0055,± 0.0007
2B21416D,1080 °C,4, 0.000015, 0.046805, 0.000001, 0.000597, 0.012181,25.50,± 9.55, 72.86, 1.56,0.0055,± 0.0010
2B21417D,1250 °C,4, 0.000383, 0.044384, 0.000009, 0.001039, 0.019864,23.91,± 8.19, 14.79, 2.71,0.0101,± 0.0019
2B21418D,1400 °C,4, 0.000194, 0.002863, 0.000001, 0.000017, 0.000800,58.83,± 472.94, 1.37, 0.04,0.0025,± 0.0050
,,,,,,,,,,,,

MQR9b,,,,,,,,,,,,

2B21429D, 580 °C,, 0.000276, 0.008096, 0.000012, 0.001268, 0.033765,33.27,± 7.08, 29.06, 3.25,0.0674,± 0.0841
2B21430D, 650 °C,, 0.000597, 0.026567, 0.000020, 0.004070, 0.061177,18.86,± 2.52, 25.54, 10.42,0.0659,± 0.0190
2B21431D, 720 °C,, 0.000821, 0.045378, 0.000041, 0.005763, 0.078157,17.03,± 3.03, 24.19, 14.76,0.0546,± 0.0120
2B21432D, 800 °C,, 0.000708, 0.044088, 0.000063, 0.005874, 0.072571,15.52,± 2.22, 25.55, 15.04,0.0573,± 0.0115
2B21433D, 850 °C,, 0.000227, 0.016162, 0.000025, 0.002448, 0.018105,9.31,± 3.23, 21.05, 6.27,0.0651,± 0.0286
2B21434D, 925 °C,, 0.000100, 0.023210, 0.000017, 0.002665, 0.011248,5.32,± 2.17, 27.27, 6.82,0.0494,± 0.0148
2B21435D,1000 °C,, 0.001084, 0.255197, 0.000073, 0.007720, 0.096467,15.69,± 2.90, 22.97, 19.77,0.0130,± 0.0017
2B21436D,1020 °C,, 0.000430, 0.105704, 0.000017, 0.003198, 0.046897,18.40,± 3.21, 26.74, 8.19,0.0130,± 0.0018
2B21437D,1040 °C,, 0.000429, 0.191704, 0.000028, 0.003556, 0.050580,17.85,± 2.49, 28.32, 9.11,0.0080,± 0.0011
2B21438D,1060 °C,, 0.000120, 0.109210, 0.000000, 0.001201, 0.018893,19.73,± 5.01, 34.44, 3.08,0.0047,± 0.0007
2B21439D,1080 °C,, 0.000064, 0.079762, 0.000000, 0.000744, 0.014098,23.74,± 8.61, 42.48, 1.91,0.0040,± 0.0007
2B21440D,1250 °C,, 0.000219, 0.054174, 0.000004, 0.000537, 0.008664,20.26,± 14.17, 11.72, 1.37,0.0043,± 0.0007
2B21441D,1400 °C,, 0.000090, 0.005465, 0.000011, 0.000009, 0.001957,263.76,± 1195.55, 6.77, 0.02,0.0007,± 0.0015

,,,,,,,,,,,,

W2.2,,,,,,,,,,,,

0B9717D, 550 °C,4, 0.000619, 0.059846, 0.000011, 0.010886, 0.199962,24.06,± 1.63, 52.22, 5.05,0.078,± 0.005
0B9719D, 700 °C,, 0.002859, 0.486387, 0.000000, 0.056231, 1.112922,25.91,± 0.72, 56.84, 26.07,0.050,± 0.003
0B9720D, 775 °C,4, 0.000698, 0.221743, 0.000041, 0.031866, 0.621645,25.55,± 0.65, 75.08, 14.77,0.062,± 0.003
0B9721D, 850 °C,4, 0.000696, 0.147240, 0.000051, 0.016667, 0.321567,25.27,± 0.99, 60.98, 7.73,0.049,± 0.003
0B9722D, 925 °C,4, 0.000764, 0.145497, 0.000091, 0.014283, 0.269816,24.74,± 1.17, 54.44, 6.62,0.042,± 0.002
0B9723D,1000 °C,4, 0.000991, 0.167293, 0.000125, 0.016104, 0.289108,23.52,± 1.10, 49.69, 7.47,0.041,± 0.002
0B9724D,1075 °C,4, 0.001801, 0.255471, 0.000247, 0.030868, 0.576182,24.45,± 0.83, 51.99, 14.31,0.052,± 0.003
0B9725D,1150 °C,4, 0.003315, 2.017123, 0.000549, 0.031376, 0.575496,24.03,± 1.54, 37.01, 14.55,0.007,± 0.000
0B9726D,1225 °C,4, 0.000899, 1.151679, 0.000024, 0.006500, 0.120725,24.33,± 4.11, 31.26, 3.01,0.002,± 0.000
0B9727D,1300 °C,4, 0.001500, 0.081983, 0.000008, 0.000904, 0.011745,17.06,± 24.96, 2.58, 0.42,0.005,± 0.000

,,,,,,,,,,,,

20b,,,,,,,,,,,,

0B11922D, 600 °C,4, 0.000190, 0.104684, 0.000868, 0.019879, 0.441653,28.70,± 0.88, 88.70, 13.84,0.082,± 0.006
0B11923D, 650 °C,4, 0.000236, 0.127378, 0.000649, 0.020482, 0.443132,27.95,± 0.85, 86.38, 14.26,0.069,± 0.005
0B11924D, 700 °C,4, 0.000232, 0.123740, 0.000514, 0.016790, 0.368785,28.37,± 0.93, 84.32, 11.69,0.058,± 0.004
0B11925D, 775 °C,4, 0.000514, 0.165016, 0.000787, 0.020445, 0.435734,27.54,± 0.79, 74.15, 14.24,0.053,± 0.003
0B11926D, 850 °C,4, 0.000286, 0.122051, 0.001113, 0.013832, 0.285505,26.68,± 1.18, 77.16, 9.63,0.049,± 0.003

0B11927D, 925 °C,, 0.000167, 0.091609, 0.001772, 0.009580, 0.179695,24.26,± 1.37, 78.46, 6.67,0.045,± 0.003
0B11928D,1000 °C,, 0.000277, 0.135225, 0.002945, 0.010595, 0.201626,24.61,± 1.40, 71.13, 7.38,0.034,± 0.002
0B11929D,1075 °C,, 0.000628, 0.800761, 0.004919, 0.011040, 0.221704,25.96,± 1.73, 54.43, 7.69,0.006,± 0.000
0B11930D,1150 °C,, 0.000517, 2.209362, 0.002873, 0.018101, 0.384799,27.47,± 2.00, 71.57, 12.60,0.004,± 0.000
0B11931D,1225 °C,, 0.000501, 0.184947, 0.000099, 0.002825, 0.052808,24.18,± 5.94, 26.28, 1.97,0.007,± 0.000
0B11932D,1300 °C,, 0.000977, 0.004876, 0.000026, 0.000053, 0.000000,0.00,± 0.00, 0.00, 0.04,0.005,± 0.003

,,,,,,,,,,,,

WS1.1 ,,,,,,,,,,,,

4B31832D, 540 °C,,0.0000047,0.0023699,0.0000054,0.0010005,0.0127194,15.13,± 7.70, 89.97, 1.12,0.1815,± 0.1355
4B31833D, 580 °C,,0.0000142,0.0033136,0.0000048,0.0012582,0.0135828,12.86,± 6.22, 76.22, 1.41,0.1633,± 0.0805
4B31834D, 620 °C,4,0.0000711,0.0106317,0.0000000,0.0024700,0.0184357,8.90,± 3.15, 46.46, 2.76,0.0999,± 0.0194
4B31835D, 660 °C,4,0.0000967,0.0183095,0.0000061,0.0035430,0.0272339,9.16,± 2.44, 48.55, 3.96,0.0832,± 0.0108
4B31836D, 700 °C,4,0.0001842,0.0284961,0.0000015,0.0049875,0.0285710,6.83,± 1.71, 34.19, 5.58,0.0753,± 0.0078
4B31837D, 740 °C,4,0.0002561,0.0380037,0.0000144,0.0072984,0.0513970,8.40,± 1.33, 40.20, 8.17,0.0826,± 0.0081
4B31838D, 780 °C,4,0.0003227,0.0440319,0.0000097,0.0080628,0.0545872,8.07,± 1.23, 36.17, 9.02,0.0787,± 0.0087
4B31839D, 820 °C,4,0.0002557,0.0462401,0.0000145,0.0075266,0.0493638,7.82,± 1.22, 39.26, 8.42,0.0700,± 0.0078
4B31840D, 900 °C,4,0.0002203,0.0709756,0.0000058,0.0087418,0.0497373,6.79,± 1.05, 43.06, 9.78,0.0530,± 0.0051
4B31841D, 975 °C,4,0.0001047,0.0421497,0.0000311,0.0049676,0.0248182,5.96,± 1.71, 44.25, 5.56,0.0507,± 0.0052
4B31842D,1050 °C,4,0.0008321,0.1698653,0.0000597,0.0139962,0.0824204,7.02,± 1.00, 24.91, 15.66,0.0354,± 0.0030
4B31843D,1100 °C,4,0.0005274,0.2922517,0.0000463,0.0119086,0.0728588,7.30,± 1.18, 31.63, 13.32,0.0175,± 0.0015
4B31844D,1150 °C,4,0.0001854,0.6671340,0.0000216,0.0075159,0.0516506,8.19,± 1.64, 48.27, 8.41,0.0048,± 0.0004
4B31845D,1200 °C,,0.0000903,0.3222430,0.0000131,0.0032678,0.0272253,9.93,± 2.80, 50.25, 3.66,0.0044,± 0.0004
4B31846D,1300 °C,,0.0001717,0.1747024,0.0000135,0.0028347,0.0126631,5.33,± 3.31, 19.81, 3.17,0.0070,± 0.0006

,,,,,,,,,,,,

W1.1 - plag,,,,,,,,,,,,

9A7136D, 500 °C,, 0.002343, 0.000000, 0.000080, 0.001619, 0.000000,0.00,± 0.00, 0.00, 17.11,,
9A7137D, 600 °C,, 0.000846, 0.049049, 0.000001, 0.000609, 0.007243,7.28,± 11.24, 2.82, 6.44,0.005,± 0.002
9A7138D, 700 °C,, 0.000915, 0.095009, 0.000000, 0.000814, 0.034981,26.18,± 9.89, 11.45, 8.60,0.004,± 0.001
9A7139D, 800 °C,, 0.000937, 0.141286, 0.000014, 0.001312, 0.058311,27.06,± 6.37, 17.39, 13.86,0.004,± 0.001
9A7140D, 900 °C,, 0.000849, 0.104417, 0.000033, 0.001003, 0.047958,29.09,± 8.13, 16.04, 10.60,0.004,± 0.001
9A7141D,1000 °C,, 0.000988, 0.023662, 0.000009, 0.000377, 0.019259,31.03,± 24.61, 6.19, 3.99,0.007,± 0.004
9A7142D,1100 °C,, 0.001507, 0.039877, 0.000007, 0.000463, 0.030096,39.47,± 24.65, 6.33, 4.89,0.005,± 0.002
9A7143D,1200 °C,, 0.000467, 0.013139, 0.000000, 0.000181, 0.013844,46.20,± 39.54, 9.12, 1.92,0.006,± 0.005

9A7144D,1350 °C,, 0.001128, 0.030074, 0.000000, 0.000267, 0.032499,73.17,± 35.13, 8.88, 2.82,0.004,± 0.002
9A7145D,1500 °C,, 0.003083, 0.303072, 0.000023, 0.002819, 1.009008,207.17,± 8.49, 52.55, 29.79,0.004,± 0.000
,,,,,,,,,,,,
W3.4 - plag,,,,,,,,,,,,
9B7310D, 500 °C,, 0.000358, 0.019493, 0.000044, 0.000510, 0.000000,0.00,± 0.00, 0.00, 5.01,0.011,± 0.011
9B7311D, 600 °C,, 0.000089, 0.052990, 0.000000, 0.000423, 0.011356,16.64,± 9.51, 30.07, 4.15,0.003,± 0.001
9B7312D, 700 °C,, 0.000083, 0.077479, 0.000004, 0.000782, 0.026582,21.04,± 8.12, 52.03, 7.68,0.004,± 0.001
9B7313D, 800 °C,4, 0.000058, 0.128577, 0.000000, 0.001429, 0.065197,28.18,± 4.92, 79.32, 14.04,0.005,± 0.001
9B7314D, 900 °C,4, 0.000039, 0.183536, 0.000021, 0.001916, 0.095277,30.68,± 5.50, 89.29, 18.83,0.004,± 0.001
9B7315D,1000 °C,4, 0.000051, 0.130795, 0.000013, 0.001580, 0.076761,30.00,± 2.48, 83.47, 15.52,0.005,± 0.001
9B7316D,1100 °C,4, 0.000238, 0.082377, 0.000011, 0.001227, 0.056047,28.20,± 7.24, 44.33, 12.06,0.006,± 0.002
9B7317D,1200 °C,4, 0.000065, 0.029994, 0.000002, 0.000325, 0.019981,37.82,± 26.56, 51.03, 3.20,0.005,± 0.005
9B7318D,1300 °C,4, 0.000202, 0.021798, 0.000000, 0.000264, 0.006432,15.09,± 31.00, 9.73, 2.59,0.005,± 0.005
9B7319D,1370 °C,4, 0.000079, 0.010776, 0.000000, 0.000363, 0.024666,41.85,± 16.45, 51.40, 3.56,0.014,± 0.024
9B7320D,1440 °C,4, 0.000135, 0.071414, 0.000011, 0.000725, 0.040075,34.08,± 8.26, 50.05, 7.12,0.004,± 0.001
9B7321D,1520 °C,4, 0.000168, 0.065121, 0.000007, 0.000635, 0.029088,28.29,± 8.08, 36.99, 6.24,0.004,± 0.001
,,,,,,,,,,,,
WS1.3 - plag,,,,,,,,,,,,
9B7528D, 550 °C,, 0.000000, 0.000000, 0.000000, 0.000000, 0.000000,0.00,± 0.00, 0.00, 0.00,,
9B7529D, 550 °C,, 0.000000, 0.000000, 0.000000, 0.000000, 0.000000,0.00,± 0.00, 0.00, 0.00,0.000,± 0.000
9B7530D, 620 °C,, 0.000017, 0.000000, 0.000013, 0.000036, 0.000000,0.00,± 0.00, 0.00, 0.64,,
9B7531D, 700 °C,, 0.000022, 0.000000, 0.000004, 0.000062, 0.000000,0.00,± 0.00, 0.00, 1.10,0.003,± 0.005
9B7532D, 800 °C,, 0.000030, 0.008458, 0.000000, 0.000122, 0.000000,0.00,± 0.00, 0.00, 2.17,0.006,± 0.012
9B7533D, 900 °C,, 0.000041, 0.022213, 0.000000, 0.000204, 0.000000,0.00,± 0.00, 0.00, 3.63,0.004,± 0.003
9B7534D,1000 °C,4, 0.000041, 0.021143, 0.000000, 0.000412, 0.003059,4.66,± 8.00, 20.02, 7.33,0.008,± 0.008
9B7535D,1100 °C,4, 0.000045, 0.042541, 0.000000, 0.000567, 0.004073,4.50,± 6.83, 23.55, 10.10,0.006,± 0.002
9B7536D,1200 °C,4, 0.000063, 0.043449, 0.000001, 0.000749, 0.004323,3.62,± 4.85, 18.74, 13.34,0.007,± 0.003
9B7537D,1300 °C,4, 0.000051, 0.059470, 0.000011, 0.000865, 0.010945,7.92,± 5.97, 42.06, 15.41,0.006,± 0.002
9B7538D,1370 °C,4, 0.000067, 0.065522, 0.000023, 0.000872, 0.008324,5.98,± 5.60, 29.62, 15.53,0.006,± 0.002
9B7539D,1440 °C,4, 0.000050, 0.058477, 0.000000, 0.000799, 0.016037,12.56,± 8.53, 52.17, 14.23,0.006,± 0.002
9B7540D,1540 °C,4, 0.000114, 0.046467, 0.000000, 0.000927, 0.011391,7.70,± 7.75, 25.32, 16.51,0.009,± 0.005
,,,,,,,,,,,,

Petrographic description of representative samples of Ogaden dyke swarm

All pictures are from optic microscopy. Upper: polarized light; lower: polarized light, crossed nicols.

MQR-8 200 µ

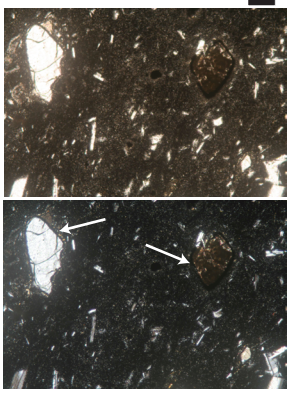

Microporphyric texture with microlites of plagioclase and abundant euhedral oxide and intersertal clinopyroxene. Numerous xenocrysts of quartz with clinopyroxene reaction rims and phantoms of amphiboles xenocrysts highly altered and destabilized in oxide (left arrow in lower left picture: quartz, right arrow: amphibole phantom).

MQR-9 200 µ

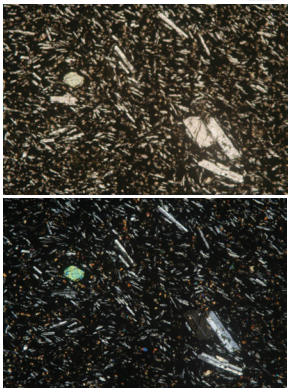

Microlitic texture with microphenocysts of plagioclase and clinopyroxene, microlites of plagioclase, and dendritic oxides.

MAO-3 200 µ

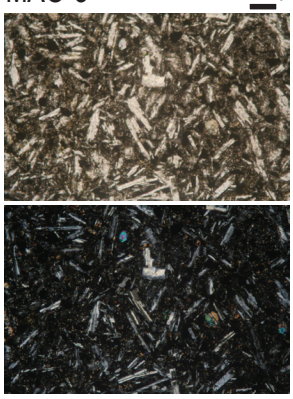

Microlitic texture with plagioclase microlites, intersertal clinopyroxenes, dendritic oxides, and olivines. Olivine locally displays minor alteration in serpentine minerals. Few quartz grains with pyroxene reaction rims.

42.1 200 µ

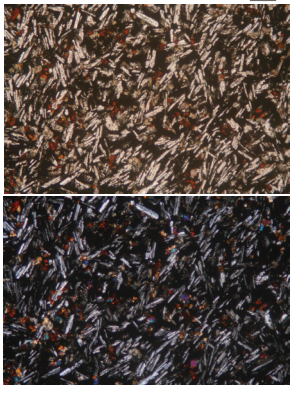

Microlitic texture with plagioclase microlites and acicular oxide, partially alterered intersertal clinopyroxene (red-brown color upper left picture). Corroded quartz grains with pyroxene reaction rims.

41a 200 µ

Microlitic texture with plagioclase microliths and acicular oxide, interstitial clinopyroxene and oxides weakly altered.

11b 200 µ

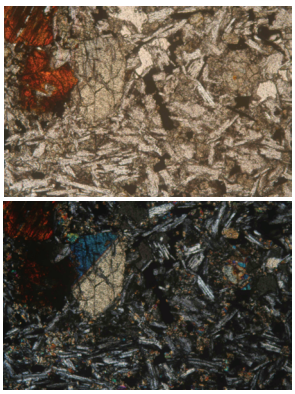

Microlitic texture with plagioclase microlite, intersertitial clinopyroxene and oxide, microphenocrysts of partially altered clinopyroxene (red-brown color in upper left figure).

4 200 µ

Microlitic texture with plagioclase microlite, partially alterered intersertal clinopyroxene (red-brown color in upper left figure), microphenocrysts of opaque and clinopyroxenes.

Major and trace analyses of georeferenced materials BCR-2 for the Ogaden Dyke Swarm samples

	BCR2			MQR8	
	Average(N=4)	%RSD	rec. value	Average (N=4)	%RSD
SiO2 (wt. %)	53,91	0,5	54,1	51,10	0,3
TiO2	2,29	0,9	2,26	2,67	2,6
Al2O3	13,40	0,4	13,5	14,07	0,7
Fe2O3T	13,86	0,8	13,8	12,86	1,2
MnO	0,198	1,2		0,182	1,4
MgO	3,62	1,2	3,59	5,83	0,6
CaO	7,12	0,8	7,12	9,87	0,8
Na2O	3,13	1,0	3,16	2,48	0,6
K2O	1,78	0,7	1,79	0,34	1,7
P2O5	0,355	0,8	0,35	0,336	0,8
Sc (ppm)	32,68	1,4	33,00	30,78	0,3
V	411	0,5	416	369	0,8
Cr	16,8	3,7	18,0	96,8	1,2
Co	36,4	0,8	37,0	45,6	1,0
Ni	12	4,5	-	54	0,6
Cu	19	1,1	19	41	0,6
Zn	129	1,1	127	109	1,3
Rb	47	0,6	48	6	0,6
Sr	337	1,8	346	379	0,5
Y	37,0	0,2	37,0	27,9	0,5
Zr	193	1,8	188	160	2,3
Nb	13	0,7	-	17	1,3
Cs	1,14	1,4	1,10	0,10	1,4
Ba	674	2,5	683	197	0,3
La	24,8	0,4	25,0	16,1	0,5
Ce	52,6	0,3	53,0	37,3	0,2
Pr	6,82	1,4	6,80	5,18	0,8
Nd	28,6	1,5	28,0	22,8	1,2
Sm	6,56	0,7	6,70	5,49	1,1
Eu	1,93	1,0	2,00	1,88	1,3
Gd	6,76	2,6	6,80	5,74	0,7
Tb	1,05	1,6	1,07	0,89	0,4
Dy	6,40	1,3	-	5,18	1,6
Ho	1,30	0,4	1,33	1,05	0,3
Er	3,48	2,6	-	2,70	1,8
Yb	3,41	0,3	3,50	2,41	0,8
Lu	0,51	0,0	0,51	0,36	0,4
Hf	4,82	0,6	4,80	3,86	1,0
Ta	0,78	0,3	-	1,05	1,1
Th	5,76	0,6	6,20	1,50	1,3
U	1,67	1,5	1,69	0,50	1,0